

# Deletion of the deISGylating enzyme USP18 enhances tumour cell antigenicity and radiosensitivity

Adan Pinto-Fernandez<sup>1,2,8</sup>; Mariolina Salio<sup>3</sup>; Tom Partridge<sup>5</sup>; Jianzhou Chen<sup>4</sup>; George Vere<sup>1</sup>;  
Helene Greenwood<sup>1</sup>; <sup>1</sup>; Andreas Damianou<sup>1</sup>; Hannah Claire Scott<sup>1</sup>; Henry Jack Pegg<sup>7</sup>;  
Alessandra Chiarenza<sup>7</sup>; Laura Díaz-Saez<sup>1,6</sup>; Paul Smith<sup>1,6</sup>; Claudia Gonzalez-Lopez<sup>3</sup>;  
Bhavisha Patel<sup>7</sup>; Emma Anderton<sup>7</sup>; Neil Jones<sup>7</sup>; Tim R. Hammonds<sup>7</sup>; Kilian Huber<sup>1,6</sup>; Ruth  
Muschel<sup>4</sup>; Persephone Borrow<sup>5</sup>; Vincenzo Cerundolo<sup>3</sup> and Benedikt M. Kessler<sup>1,2,8</sup>

<sup>1</sup>TDI Mass Spectrometry Laboratory, Target Discovery Institute, Nuffield Department of Medicine,  
University of Oxford, Oxford, Roosevelt Drive, Oxford OX3 7FZ, UK

<sup>2</sup>Chinese Academy of Medical Sciences Oxford Institute, Nuffield Department of Medicine,  
University of Oxford, Oxford, Roosevelt Drive, Oxford OX3 7FZ, UK

<sup>3</sup>MRC Human Immunology Unit, MRC Weatherall Institute of Molecular Medicine, Radcliffe  
Department of Medicine, University of Oxford, Oxford OX3 9DS, UK

<sup>4</sup>CRUK/MRC Oxford Institute for Radiation Oncology, Department of Oncology, University of  
Oxford, Oxford, OX3 7DQ, UK

<sup>5</sup>Nuffield Department of Clinical Medicine, University of Oxford, Roosevelt Drive, Oxford OX3  
7FZ, UK

<sup>6</sup>Structural Genomics Consortium, Nuffield Department of Medicine, University of Oxford, Oxford,  
Roosevelt Drive, Oxford OX3 7FZ, UK

<sup>7</sup>CRUK Therapeutic Discovery Laboratories, London Bioscience Innovation Centre, London, NW1  
0NH, UK

**Running Title:** New roles for USP18 in cancer therapy

## <sup>8</sup>Corresponding authors:

Adan Pinto-Fernandez  
Target Discovery Institute  
Nuffield Department of Medicine  
University of Oxford  
Oxford OX3 7FZ, UK  
Email: adan.pintofernandez@ndm.ox.ac.uk

Benedikt M. Kessler  
Target Discovery Institute  
Nuffield Department of Medicine  
University of Oxford  
Oxford OX3 7FZ, UK  
Email: benedikt.kessler@ndm.ox.ac.uk

## 50 **Abstract**

## 51 **Background**

52 Interferon (IFN) signalling pathways, a key element of the innate immune response,  
53 contribute to resistance to conventional chemotherapy, radiotherapy, and  
54 immunotherapy, and are often deregulated in cancer. The deubiquitylating enzyme  
55 USP18 is a major negative regulator of the IFN signalling cascade and is the  
56 predominant human protease that cleaves ISG15, a ubiquitin-like protein tightly  
57 regulated in the context of innate immunity, from its modified substrate proteins *in vivo*.

## 58 **Methods**

59 In this study, using advanced proteomic techniques, we have significantly expanded the  
60 USP18-dependent ISGylome and proteome in a chronic myeloid leukaemia (CML)-  
61 derived cell line. USP18-dependent effects were explored further in CML and colorectal  
62 carcinoma cellular models.

## 63 **Results**

64 Novel ISGylation targets were characterised that modulate the sensing of innate ligands,  
65 antigen presentation and secretion of cytokines. Consequently, CML USP18-deficient  
66 cells are more antigenic, driving increased activation of cytotoxic T lymphocytes (CTLs)  
67 and are more susceptible to irradiation.

## 68 **Conclusions**

69 Our results provide strong evidence for USP18 in regulating antigenicity and  
70 radiosensitivity, highlighting its potential as a cancer target.

## 71 **Background**

72 Despite its clinical success in inducing regression of certain tumours, immune-  
73 checkpoint blockade (ICB) therapy is limited by being effective in only a fraction of  
74 patients. Many patients develop resistance (1) to treatment; Moreover, ICB frequently  
75 has profound side effects, including pneumonitis and other autoimmune related adverse  
76 events (irAEs) (2), calling for the discovery of predictive biomarkers of ICB success and  
77 for novel ways to boost ICB therapy further. Numerous studies point towards defects in  
78 interferon-dependent pattern recognition pathways (3-5) and the antigen-presentation  
79 pathway (6, 7) as the main resistance mechanisms tumour cells use to avoid the  
80 immune system and to escape the effects of immunotherapy (8, 9). In addition to the  
81 roles of elements of the innate immune response in modulating the efficacy of cancer  
82 immunotherapy, it has also been reported that radiotherapy promotes the expression of  
83 interferon-stimulated genes (ISGs) that are involved in resistance to ionizing irradiation  
84 (10). Immunomodulatory imide drugs (IMiDs) such as thalidomide analogues are another  
85 category of immunomodulators that are routinely used to treat patients with multiple  
86 myeloma and also lead to increased expression of ISGs (11). Therefore, there is strong  
87 evidence pointing at the innate immune response as a resistance mechanism that  
88 cancer cells use to survive the effects of immune checkpoint blockade and other cancer  
89 therapies.

90 One of the main regulators of the innate immune response is the deISGylating enzyme  
91 USP18 (Fig.1A). Despite its full name (ubiquitin-specific protease 18), USP18 is not a  
92 deubiquitylating enzyme (DUB). In fact, it is the predominant protease described to date  
93 to recognise and to remove specifically the ubiquitin-like protein ISG15 from modified  
94 proteins *in vivo*. USP2, USP5, USP13, USP14, and USP21 DUBs are also active in  
95 ISG15 *in vitro* assays, but they do not seem to deconjugate ISG15 in a cellular context  
96 (12-15).

97 ISG15 is structurally very similar to a dimer of ubiquitin, and its expression is, like that of  
98 USP18, tightly regulated by type I IFN. Both ISG15 and USP18 contribute to innate

99 immune responses and are important in other cellular processes such as autophagy and  
100 protein translation (16). ISG15 is not conserved across species and its functions may  
101 vary between organisms. It has been identified only in vertebrates; moreover, human  
102 and murine ISG15 protein sequences only share 64% and 74% homology and similarity,  
103 respectively (17).

104 *Usp18*<sup>-/-</sup> mice present a strong accumulation of ISG15 conjugates in tissues as well as a  
105 prolonged increase in STAT1-dependent activation (18). These mice are hypersensitive  
106 to IFN and Poly I:C (a synthetic double-stranded RNA) stimulation, and are more  
107 resistant to intracerebral infection. In some mice genetic backgrounds, *Usp18* deficiency  
108 has been linked to brain abnormalities (15, 18, 19).

109 USP18 functions that are independent of ISG15 seem to be crucial in mice since the  
110 phenotype observed in *Usp18*<sup>-/-</sup> animals, including brain inflammation and de-regulated  
111 STAT1 signalling, cannot be rescued by *Isg15* depletion (20). In humans, however, free  
112 ISG15 stabilises USP18 and acts as a negative regulator of the IFN pathway (21, 22).  
113 ISG15-null patients present with inflammation due to deregulation of the type I interferon  
114 response and, interestingly, are susceptible to mycobacterial, but not viral, diseases (21,  
115 23).

116 It has also been reported that silencing USP18 increases surface expression of peptide-  
117 loaded MHC-II (24), supporting its role as a negative regulator of immunogenicity.  
118 USP18 has been linked to cancer development, being overexpressed in lung, colon,  
119 pancreas and breast cancer, but also associated with autoimmune diseases, and  
120 neuroinflammation (15, 25-27). Notably, USP18 has also been described to have a role  
121 as a resistance factor to traditional chemotherapy agents Bortezomib and Mafosfamide  
122 in tumour cells (28, 29), suggesting that its inhibition may serve as a boost for such  
123 therapies.

Protein ISGylation profiles in human cells have been previously reported, but with limited depth and predominantly based on overexpression systems (30-35). To obtain deep coverage and modified residue information in a more physiologically relevant context, we decided to combine advanced proteomic techniques with the immunoaffinity purification of GlyGly tryptic peptides (36) in wild-type (WT) and USP18 <sup>-/-</sup> knockout (KO) HAP1 cells, in order to analyse the first USP18-dependent ISGylome of human cancer cells.

## Methods

### Cell lines and T cells

Chronic myeloid leukaemia (CML)-derived HAP1 wild-type (WT; Horizon #C631) cells and HAP1 USP18<sup>-/-</sup> (KO; Horizon #HZGHC000492c011) were a kind gift from the laboratory of Sebastian Nijman and were cultured in IMDM media (Gibco #12440-53) supplemented with 10% FBS (Gibco #10500-64) at 37 °C in a humidified 5% CO<sub>2</sub> atmosphere. HAP1 USP18 KO cells were generated by editing parental HAP1 cells with CRISPR/Cas9 to contain a 4bp deletion in the coding exon 3 of the *USP18* gene. Melan-A specific CTL lines were isolated from healthy blood donors as described (37). Colorectal carcinoma-derived HCT116 wild-type (ATCC-CCL-247) and HCT116 USP18 KO were cultured in DMEM media (Gibco #10313) supplemented with 10% FBS (Gibco #10500-64) at 37 °C in a humidified 5% CO<sub>2</sub> atmosphere. HCT116 KO cells were generated using the commercially available USP18 CRISPR/Cas9 KO (Santa Cruz #sc-402259) and USP18 homology-directed DNA repair HDR (Santa Cruz #sc-402259-HDR) plasmids, following the manufacturer's recommendations. PBMC were isolated from healthy blood purchased through the UK National Blood Service (agreement T293). Briefly, dendritic cells pulsed with Melan A peptides (ELA<sub>26-35</sub> ELAGIGILTV, Sigma) were incubated with autologous PBMC; after 12 days melan-A specific CD8 T cells were sorted with HLA-A2-ELA class I tetramers and expanded.

### Stimulation of cells

150 Cells were treated with 1000 U/mL of human interferon alpha 2 (Alpha2b) from PBL  
151 Assay Science (Cat. No. 11105-1) for the indicated times.

#### 152 **DNA plasmids and generation of stable cell lines**

153 The Flag-HA-USP18WT construct was purchased from Addgene (#22572) and the Flag-  
154 HA-USP18C64R/C65R construct was generated using the Q5® Site-Directed  
155 Mutagenesis Kit (NEB, E0554S) and the primers OL87:  
156 TGGACAGACCcggcggCTTAACCTCTTG and OL88: ATGTTGTGTAAACCAACC.  
157 Primers were designed using the NEBaseChanger online tool:  
158 <http://nebasechanger.neb.com/> and the successful clone confirmed by sequencing  
159 (Eurofins).

160 Transfected HAP1 and HCT116 cells were selected, pooled, and subsequently cultured  
161 in growth media supplemented with puromycin (Gibco) at 1 µg/mL.

#### 162 **siRNA reagents**

163 ISG15 siRNA on-TARGET plus SMART plus (Dharmacon #L-004235-03-0005) and  
164 ADAR siRNA on-TARGET plus SMART plus (Dharmacon #L-008630-00-0005).

#### 165 **Cell transfection**

166 USP18 cDNA, CRISPR/Cas9, and HDR plasmids were transfected with Lipofectamine  
167 LTX and Plus (Invitrogen #15338-100) following the manufacturer's instructions. The  
168 indicated siRNA sequences were transfected with Lipofectamine RNAimax (Invitrogen  
169 #13778-150) following the manufacturer's instructions.

#### 170 **Antibodies**

Antibody	Application	Brand	Cat. No.
USP18	Immunoblot / Immunofluorescence	Cell Signaling -CST	4813
ISG15	Immunoblot / Immunofluorescence	CST	2743
ISG15	Immunoprecipitation	Boston Biochem	A-830
Ubiquitin (Ubisite)	Immunoblot	Millipore	MAB5486
NEDD8	Immunoblot	CST	2745
dsRNA	Immunofluorescence	Millipore	MABE1134
ADAR	Immunoblot	CST	14175
phospho STAT1 (Y701)	Immunofluorescence	CST	9167
HERC5	Immunoblot	Invitrogen	703675
IFIT3	Immunoblot	Abcam	ab76818
PKR	Immunoblot	CST	12297
Phosphor PKR (T446)	Immunoblot	Abcam	ab32036
IFN $\gamma$	ELISA	BD	555142
PDL1	FACS	Biologend	Clone 29E.2A3
HLA-A2	FACS	Biologend	Clone BB7.2
CD25	FACS	BD	Clone M-A251
CD137	FACS	Biologend	Clone 4B4-1

171

## 172 Western blotting

173 Cells were washed with ice-cold PBS and lysed with NP-40 lysis buffer (50 mM Tris pH  
174 7.4, 0.5% (v/v) NP40, 150 mM NaCl and 20 mM MgCl<sub>2</sub>) buffer containing protease and  
175 phosphatase inhibitors. For Western blotting, 25  $\mu$ g of protein was then fractionated on  
176 Tris–glycine SDS-PAGE gradient (4–15% acrylamide) gels (BioRad; #3450123),  
177 transferred onto PVDF membranes (Millipore; IPFL00010), and detected with the  
178 indicated antibodies using a LI-COR detection system.

## 179 USP18 ABP

180 ISG15-PA was synthesised in the Kessler lab using the ISG15 C-term (79-156) construct  
181 from Addgene (#110760) and DUB ABP assays were performed as previously described  
182 (38). Briefly, HAP1 cells were lysed in glass beads lysis buffer (GBL: 50 mM Tris, pH 7.5,  
183 5 mM MgCl<sub>2</sub>, 0.5 mM EDTA, and 250 mM Sucrose) and the extracts were labelled with  
184 ISG15-PA for 45 min at 37°C, and immunoblotted with specific anti-USP18 antibodies.

## 185 Cell growth, morphology and proliferation assays

186 10000 cells were seeded in 6-well or 12-well plates and cell were imaged in an IncuCyte  
187 Zoom Imager (Essen Bioscience) for live-cell imaging during the indicated times at the

188 indicated intervals the phase contrast channel. Cell growth was determined by  
189 measuring the percent confluence over time. End point cell viability was measured using  
190 the Resazurin assay (Alamar Blue; Thermo Fisher #DAL1025), following the  
191 manufacturer's instructions.

## 192 **Immunofluorescence microscopy**

193 HAP1 control or HAP1 USP18 KO cells were seeded in fluorescence compatible 96 well  
194 plates (Corning), treated with IFN for the indicated times, subsequently washed with  
195 PBS, fixed using 4% paraformaldehyde (sc-281692, ChemCruz) for 10 minutes,  
196 permeabilised using 100% methanol for 10 minutes at -20 °C, and blocked with 5 % BSA  
197 in PBS for one hour at room temperature. The primary antibodies were diluted in PBST  
198 (PBS + 0.05 % Tween20) in the following concentrations: USP18 (1:100), ISG15 (1:100)  
199 and pSTAT1 (1:400), added and incubated overnight at 4 °C. Cells were then washed  
200 with PBST and subsequently incubated with secondary antibody mix consisting of Goat  
201 anti-rabbit conjugated alexa-647 (1:10000) and 4',6'-diamidino-2-phenylindole (Dapi)  
202 (2.5 µg/mL), for 1 hour at room temperature. Plates were imaged using the Opera  
203 Phenix imaging platform (Perkin Elmer).

204 For dsRNA analysis, the same workflow was used with the exception of the cells, that  
205 were fixed and permeabilised using Cytofix/Cytoperm buffers (BD biosciences), following  
206 the manufacturer's instructions. dsRNA antibody was used at a 1:100 dilution and the  
207 secondary donkey anti-mouse at a 1:500 dilution.

## 208 **Identification of ISGylated proteins using GlyGly peptidomics and matching** 209 **proteomics**

210 HAP1 lysates were used for GlyGly immunoprecipitation using the PTMScan Ubiquitin  
211 Remnant Motif Kit (Cell Signaling), according to manufacturer's protocol (36). Briefly, 20  
212 mg of extracts were solubilized and denatured in 10 mL lysis buffer (20 mM HEPES, pH  
213 8.0, 9 M urea, 1 mM sodium orthovanadate, 2.5 mM sodium pyrophosphate, 1 mM  $\beta$ -

glycerophosphate), reduced using dithiothreitol (4.5 mM final) for 30 minutes at 55 °C. This was followed by alkylation using iodoacetamide (100 mM final) for 15 minutes at room temperature in the dark. Samples were subsequently diluted fourfold in 20 mM HEPES, pH 8.0 (~2 M urea final), followed by digestion with trypsin-TPCK (Worthington, LS003744, 10 mg/mL final) overnight at room temperature. Samples were then acidified using trifluoroacetic acid (1% final), and desalted using C-18 Sep-Pak (Waters) cartridges according to the manufacturer's protocol. At this point, 20 µg of digested protein were separated for matching proteome control analysis. Peptides were lyophilized and re-suspended in 1.4 mL immunoprecipitation IAP buffer (PTMScan), and the remaining insoluble material cleared by centrifugation and anti-GlyGly antibody beads added followed by rotation and kept 4°C for 2 hours. Beads were subsequently washed twice using 1 mL IAP buffer, followed by three water washes. Immunoprecipitated material was eluted twice in 55 and 50 µL 0.15 % trifluoroacetic acid in water. Peptide material was desalted and concentrated using C-18 Sep-Pak (Waters) cartridges according to the manufacturer's protocol. Purified GlyGly-modified peptide eluates and matching proteome material were dried by vacuum centrifugation, and re-suspended in buffer A (98 % MilliQ-H<sub>2</sub>O, 2 % CH<sub>3</sub>CN and 0.1 % TFA).

### **ISG15 interactome immunoprecipitation**

HAP1 cells were lysed with Co-IP lysis buffer (20 mM Hepes pH 8.0, 150 mM NaCl, 0.2 % NP-40, 10 % Glycerol, 5 mM NEM, phosphatase and protease inhibitor cocktails (25 x 10<sup>6</sup> cells per condition) and subjected to immunoprecipitation using 5 µg of ISG15 antibody (Boston Biochem #A-380) plus 25 µL of protein G Sepharose slurry (Invitrogen; #15920-10), for 16 hours at 4 °C. Beads were washed 4 times with Co-IP lysis buffer and immunocomplexes were eluted with 2X Laemmli. 10 % of the eluates was used for immunoblotting with the indicated antibody. The remaining eluate was prepared for MS analysis as previously described (38). Briefly: immunoprecipitated sample eluates were diluted to 175 µL with ultra-pure water and reduced with 5 µL of DTT (200 mM in 0.1 M

241 Tris, pH 7.8) for 30 min at 37 °C. Samples were alkylated with 20 µL of iodoacetamide  
242 (100 mM in 0.1 M Tris, pH 7.8) for 15 min at room temperature (protected from light),  
243 followed by protein precipitation using a double methanol/chloroform extraction method.  
244 Protein samples were treated with 600 µL of methanol, 150 µL of chloroform, and 450 µL  
245 of water, followed by vigorous vortexing. Samples were centrifuged at 17000 g for 3 min,  
246 and the resultant upper aqueous phase was removed. Proteins were pelleted following  
247 the addition of 450 µL of methanol and centrifugation at 17000 g for 6 min. The  
248 supernatant was removed, and the extraction process was repeated. Following the  
249 second extraction process, precipitated proteins were re-suspended in 50 µL of 6 M urea  
250 and diluted to <1 M urea with 250 µL of 20 mM HEPES (pH 8.0) buffer. Protein digestion  
251 was carried out by adding trypsin (from a 1 mg/ml stock in 1 mM HCl) to a ratio 1:100,  
252 rocking at 12 rpm and room temperature overnight. Following digestion, samples were  
253 acidified to 1 % trifluoroacetic acid and desalted on C18 solid-phase extraction cartridges  
254 (SEP-PAK plus, Waters), dried, and re-suspended in buffer A.

#### 255 **Liquid chromatography- tandem mass spectrometry (LC-MS/MS) analysis**

256 LC-MS/MS analysis was performed using a Dionex Ultimate 3000 nano-ultra high-  
257 pressure reverse-phase chromatography coupled on-line to a Q Exactive HF (GlyGly),  
258 Fusion Lumos (ISG15 interactome) or a Q Exactive (Matching proteome) mass  
259 spectrometer (Thermo Scientific) as described previously (38). In brief, samples were  
260 separated on an EASY-Spray PepMap RSLC C18 column (500 mm × 75 µm, 2 µm  
261 particle size, Thermo Scientific) over a 60 min (120 min in the case of the matching  
262 proteome) gradient of 2–35 % acetonitrile in 5 % dimethyl sulfoxide (DMSO), 0.1 %  
263 formic acid at 250 nL/min. MS1 scans were acquired at a resolution of 60000 at 200 m/z  
264 and the top 12 most abundant precursor ions were selected for high collision dissociation  
265 (HCD) fragmentation.

#### 266 **Data analysis**

267 From raw MS files, searches against the UniProtKB human sequence data base (92954  
268 entries) and label-free quantitation were performed using MaxQuant Software (v1.5.5.1).  
269 Search parameters include carbamidomethyl (C) as a fixed modification, oxidation (M)  
270 and deamidation (NQ as variable modifications, maximum 2 missed cleavages (3 for the  
271 GlyGly peptidome analysis), matching between runs, and LFQ quantitation was  
272 performed using unique peptides. Label-free interaction data analysis was performed  
273 using Perseus (v1.6.0.2), and volcano and scatter plots were generated using a t-test  
274 with permutation FDR = 0.01 for multiple-test correction and s0 = 0.1 as cut-off  
275 parameters.

276 Other graphs were generated using GraphPad PRISM 8 and Excel and for the statistical  
277 analysis, we applied two-way ANOVA tests including multiple comparison testing via the  
278 Dunnett method available through the GraphPad Prism software. P value style is  
279 GraphPad: NS, P = 0.1234, \*P = 0.0332, \*\*P = 0.0021, \*\*\*P = 0.0002, \*\*\*\*P < 0.0001.

280 Gene ontology and pathway enrichment analysis were performed using STRINGdb  
281 ([https://string-db.org/cgi/input.pl?sessionId=9clBKQVOpdjY&input\\_page\\_show\\_search=on](https://string-db.org/cgi/input.pl?sessionId=9clBKQVOpdjY&input_page_show_search=on)) and  
282 g:PROFILER (<https://biit.cs.ut.ee/gprofiler/gost>).

283 Flow cytometry data were analysed with Flowjo 10, upon gating on live singlets.

#### 284 **FACS/T cell activation pulsing with Melan-A peptides**

285 50000 HAP1 WT and USP18-/- cells (+/- IFN $\alpha$ -2a, 1000 U/mL; 24h.) were plated in 96-  
286 well plates (flat bottom, Costar) and pulsed with the indicated amounts of Melan-A  
287 peptides (ELAGIGILTV, Sigma) for 2 hours at 37C. Cells were washed three times with  
288 RPMI media (Sigma) prior to addition of melan A-specific T cells (healthy donor-derived)  
289 at a ratio 2 tumour cells: 1 immune cell for 18 hours. T cell activation (FACS) and  
290 cytokine release in the supernatant (ELISA) were analysed subsequently.

291 For FACS analysis, triplicate wells were pooled, cells were stained for 20min at room  
292 temperature with a near infrared live/dead marker (Biolegend) and then with a cocktail of  
293 titrated antibodies, 30min on ice. Samples were acquired on a BD Symphony flow  
294 cytometer.

## 295 **ELISA**

296 Enhanced ELISA plates (Corning) were coated with diluted anti-IFN $\gamma$  antibodies (2  
297  $\mu$ g/mL) in coating buffer (100 mM NaHCO<sub>3</sub>) and left overnight at 4 °C. Plates were  
298 washed 6 times with PBS / 0.01 % Tween and blocked with PBS / 10 % FCS for 2 hours  
299 at room temperature. Diluted standards and samples in PBS / 10 % FCS were added to  
300 the plate and incubated for 3 hours at 37C. Plates were washed 6 times with PBS / 0.01  
301 % Tween prior addition of biotinylated anti-cytokine detecting mAb (2  $\mu$ g/mL in PBS / 10  
302 % FCS) for 45 minutes at room temperature. Plates were then washed 8 times and  
303 avidin-peroxidase (2.5  $\mu$ g/mL in PBS / 10 % FCS. Sigma) was added for 30 minutes.  
304 Finally, plates were washed 10 times with PBS/Tween and substrate was added (o-  
305 phenylenediamine dihydrochloride tablets) and then quenched with 0.2 N sulfuric acid  
306 (Sigma) after colour appears visible. Plates were read at OD 490 nm in a microplate  
307 reader.

## 308 **Clonogenic assays after RT**

309 Cancer cells were seeded in 6-well plates and treated with a range of IR doses (D): 0-10  
310 Gy. The colonies were stained and assessed on a GelCount<sup>TM</sup> Colony Counter (Oxford  
311 Optonix Ltd). The surviving fractions (SF) were calculated and normalized to the  
312 seeding efficiency. The survival curves were fitted in Prism 8 (GraphPad) using linear  
313 quadratic model:  $\ln(SF) = -\alpha D - \beta D^2$ .

## 314 **Results**

### 315 **USP18 catalytic activity is essential for cell survival in the presence of type I IFN**

316 We decided to study the effects of type I interferon Alpha 2 (IFN $\alpha$ 2; IFN hereafter) on  
317 human HAP1 cells, a chronic myeloid leukaemia (CML)-derived cell line, in the presence  
318 or absence of the USP18 gene. Under normal culture conditions, both cell lines  
319 proliferate at the same rate (Fig. 1B). However, while the parental cells are completely  
320 insensitive to treatment with 1000 U/mL of IFN (Fig. 1C), the USP18-deficient cells stop  
321 growing after 24h (Fig. 1C and Fig. S1A) and start to die as visualised by microscope  
322 phase-contrast imaging Fig. S1B. The same results were observed using the colorectal  
323 cancer cell line HCT116, suggesting an essential role for USP18 under an innate  
324 immune stimulation context, in different cancer cell types (Fig. S2A and S2B).  
325 Interestingly, the sensitivity to IFN correlated with the expression of USP18 in three  
326 different KO clones, expressing different amounts of the protein (Fig. S2C; top panel).  
327 Supporting this phenotype, a molecular indicator of programmed cell death, the cleavage  
328 of the protein PARP, is only observed in the KO cells treated with IFN (Fig. 1D).  
329 Consistent with previous literature (15, 19), deletion of USP18 also led to the  
330 accumulation of ISG15 conjugates in our cellular model, shown as a strong smear after  
331 48 hours of treatment with IFN (Fig. 1E) and an increase in ISG15 levels and STAT1  
332 phosphorylation in immunofluorescence analysis after 24 hours of IFN stimulation (Fig.  
333 S1C). Enhancement of STAT1 phosphorylation in tyrosine 701 after USP18 deletion or  
334 depletion was also detected by immunoblotting in both, HCT116 (Fig. S2C), and HAP1  
335 (Fig. S2D) cells. Strikingly, the accumulation of ISGylated proteins is barely noticeable in  
336 HAP1 WT cells after IFN treatment (Fig. 1E).

337 USP18 functions as a negative regulator of the IFN pathway have been linked not only to  
338 its ability to remove ISG15 from proteins, but also to inhibitory protein-protein  
339 interactions with IFNAR2 and STAT2 (39). In order to evaluate the importance of USP18  
340 catalytic activity in our model, we re-expressed the wild-type (WT) protein and a  
341 catalytically inactive mutant, where we mutated the catalytic cysteine and a second  
342 adjacent cysteine (C64R/C65R), in HAP1 USP18 KO cells. Stable transfectants

343 expressing the WT protein rescued KO cells from the toxic effects of IFN (Fig. 1F and  
344 Fig. S1D) and prevented the accumulation of ISGylated proteins (Fig. 1G).  
345 Unexpectedly, and in contrast with what has been published in murine systems, re-  
346 expression of USP18 C64R/C65R did not rescue the KO cells from IFN toxicity (Fig. 1F  
347 and Fig. S1D) or from the accumulation of ISGylated proteins (Fig. 1G). As a control to  
348 evaluate the activity of the two proteins, we performed deISGylating activity assays using  
349 ISG15 activity-based probes that bind irreversibly to catalytically active USP18 and allow  
350 the visualization of the active enzyme as an increase in the molecular weight ~15 kDa  
351 (USP18 plus ISG15 probe) by immunoblotting (12). We observed that only wild-type  
352 USP18 is able to bind the activity-based probe, whereas the C64R/C65R mutant is  
353 completely inactive (Fig. 1G, middle panel). As a control for inhibition of the IFN-receptor  
354 by direct binding of WT or C64R/C65R USP18, we performed immunoblots against the  
355 ISGs HERC5, IFIT3 and ISG15. Both, WT and C64R/C65R USP18 are able to inhibit the  
356 expression of these three ISGs, although the inhibitory effect seems to be smaller for the  
357 catalytically inactive mutant (Fig. S1E), perhaps pointing at a slightly impaired ability to  
358 bind IFNAR2 or STAT2 of this mutant due to structural changes induced by the  
359 mutations.

#### 360 **USP18-dependent GlyGly peptidome/proteome reveals tumour cell ISGylome**

361 Digestion with trypsin of proteins modified either with ubiquitin, ISG15 or NEDD8 leaves  
362 a unique GlyGly motif on the modified lysine (Fig. 2A and 2B). Enriching for GlyGly-  
363 modified peptides followed by mass spectrometry (MS) analysis provides access to  
364 information on not only the prevalence/amount of the modification but also on its exact  
365 position in the protein sequence. A recent report exploited this to analyse cellular  
366 ISGylomes in mice, although using a different genetic cellular background strategy to the  
367 one used here and in the context of infection (40). In this study, we employed a similar  
368 approach to conduct the first comprehensive analysis of the USP18-dependent  
369 ISGylome in human cancer cells.

Even though GlyGly peptidomics is not specific for ISG15, we hypothesised that KO of USP18 (the main deISGylating enzyme *in vivo*) in cells should lead to accumulation of ISGylated substrates upon type I IFN stimulation that would be suitable for identification using GlyGly immunoaffinity purification of the generated tryptic peptides. To validate our hypothesis, we first wanted to verify, by immunoblotting, that ubiquitylation and NEDDylation were not affected across our four experimental conditions (HAP1 WT and USP18 KO in the presence/absence of IFN). As shown in Fig. 2C and 2D, ubiquitylation, and NEDDylation did not seem to be affected, if something, we saw a small reduction of ubiquitylated proteins in the USP18 KO cells treated with IFN. In contrast, IFN treatment of the KO cells led to a massive accumulation of conjugated ISG15 material (Fig. 2E). Based on these observations, we would expect to detect mainly the accumulated ISGylated proteins when applying the GlyGly peptidomics in these particular experimental conditions. 2341 GlyGly-modified peptides were identified in this mass spectrometry-based experiment, corresponding to 2172 protein groups. As the volcano plot in Fig. S3A shows, there are no significant changes in the comparative GlyGly peptidomes of HAP1 cells treated with and without IFN, consistent with the results from the immunoblots. However, and again in line with the gel results, following treatment of USP18 KO cells with IFN and comparison of their GlyGly peptidome to that of the WT cells (also treated with IFN), we observed a massive USP18-dependent, increase in GlyGly peptides, corresponding to 476 proteins, in the KO cells (Fig. 2F). After gene ontology/pathway enrichment analysis, we could reinforce the role of USP18 as a major regulator of the innate immune response with significant enrichment of ISG15-modified peptides for dsRNA binding and closely related proteins such as ADAR, DDX58 (RIG-I), DDX60, DHX58, OAS1/2, EIF2KA2 (PKR), IFIH1, DDX3X, DHX9, STAT1 and others that are part of innate immunity pathways. In addition, we observed a strong upregulation of ISGylated (immuno)-proteasomal subunits PSMA7, PSMB9, PSMB10, and PSME2 as well as TAP1, all of which are part of the antigen presentation pathway. Proteins involved in translation and glucose metabolism processes were also

398 represented with numerous ISGylated protein members (Fig. 2F). Interestingly, we also  
399 found that proteins from a recently published signature of interferon-stimulated genes  
400 (ISGs) expressed constitutively in a subset of cancer cell lines (5) were also strongly  
401 upregulated and represented in our ISGylome (Fig. 2F). The global proteome of the  
402 same samples was analysed in parallel (Fig. S3B, 3C, and 3D). USP18 is expressed in  
403 very low amounts when the IFN pathway is inactive and therefore, unsurprisingly, we did  
404 not detect major changes in either the proteome (Fig. S3C) or the GlyGly-peptidome  
405 (Fig. S3G) of WT cells compared to USP18 KO cells growing in unstimulated conditions.  
406 However, when the IFN pathway was activated in WT cells, we could see an enrichment  
407 of ISGs and elements from the above-mentioned cancer ISG signature (Fig. S3D). In  
408 agreement with the ISGylome data, the USP18-dependent proteome (or 'interferome') in  
409 the presence of IFN showed an even stronger upregulation of ISGs, mainly consisting of  
410 dsRNA-related enzymes, proteasome subunits, and IFITs, indicating a general activation  
411 of the interferon pathway (Fig. S3B, E, and F). Interestingly, many of the upregulated  
412 proteins in the USP18-dependent interferome overlap with a subset of factors recently  
413 identified to be upregulated in metastatic melanoma responders to ICB (41). In  
414 particular, USP18 regulates the expression and/or ISGylation status of PSME1, PSMB9,  
415 PSMB10, B2M, TAPBP, TAP1, TAP2, CBR3, STAT1, IFIT1, GBP1, GBP2, ERAP1 and  
416 MAGE, all linked to better responses to ICB therapy with PD1 inhibitors (Table S1). In  
417 line with previous literature (42, 43), when cross-comparing the USP18-dependent  
418 ISGylome and proteome (in IFN-treated cells) data sets, we could observe that in our  
419 case ISGylation is not leading to a decrease in protein levels (Fig. 2G). However, a  
420 strong regulatory ISGylation of ribosomal proteins, proteasomal subunits, and some  
421 RNA-related enzymes was observed without affecting their expression, (Fig. 2G; in  
422 green) and an accumulation of modified proteins, mainly ISGs (Fig. 2G; in blue). The  
423 latter effect may putatively not be due to ISGylation leading to a stabilisation of proteins,  
424 but might instead reflect the roles of USP18 as an inhibitor of late-stage IFN signalling.

425 However, the potential role of ISG15 as stabiliser of a certain set of ISGs cannot be  
426 excluded at this point (43).

427 **USP18 controls ISGylation of the dsRNA modifier ADAR (p150) and the innate**  
428 **ligand sensor PKR and regulates their activity**

429 To verify these results, we performed immunoblotting with specific antibodies against a  
430 group of selected ISGylated hits such as ADAR, PKR, HERC5, and IFIT3, and we could  
431 observe additional bands for these proteins (consistent with, at least, an increase in the  
432 MW of ~15 kDa) only in the KO cells treated with IFN (Fig. 3A and 3D). ISGylated  
433 HERC5 material was also detected in the colorectal cancer cell line (Fig. S2C). To  
434 further validate ISGylation as the observed modification, we silenced the ISG15 gene  
435 using specific siRNA sequences in the USP18-deficient cells and we treated them with  
436 IFN. As predicted, the amount of modified ADAR (p150) was significantly reduced after  
437 partial silencing of ISG15 (Fig. 3B). As the ultimate validation technique for our GlyGly-  
438 based ISGylome, we decided to perform a classic interactome analysis after  
439 immunoaffinity purification (IAP-MS) of endogenous ISG15 proteins in the same  
440 experimental conditions. After optimisation of the immunoprecipitation (IP) conditions, we  
441 could efficiently purify ISG15 and its conjugated substrates (Fig. 3C). Again, we did not  
442 observe an increase of ubiquitylated proteins in the inputs, and we did not co-  
443 immunoprecipitate ubiquitin or ubiquitylated proteins together with ISG15 (Fig. 3C, lower  
444 panel). In the same IP eluates, we observed an enrichment of modified HERC5, ADAR,  
445 PKR and IFIT3, all ISGylated in the GlyGly data, in the USP18 KO cells treated with IFN  
446 (Fig. 3D). Mass spectrometry analysis of the eluates showed enrichment of very similar  
447 proteins to the matching GlyGly peptidome in the USP18 KO cells treated with IFN (Fig.  
448 3E). From a total of 312 ISGylated proteins found to interact with ISG15 in a USP18-  
449 dependent manner, 110 proteins overlapped when comparing the two techniques (Fig.  
450 S4A), primarily the ones showing a stronger enrichment in the volcano plot in Fig. 3E  
451 (highlighted and labelled in green) and in the comparative scatter (ISG15 interactome

452 *versus* GlyGly peptidome) plot in Fig. 3F, upper right area. These complementary  
453 experiments validated our approach for analysis of the site-specific ISGylome using  
454 GlyGly peptidomics.

455 The double-stranded RNA-specific adenosine deaminase ADAR (adenosine deaminase  
456 acting on RNA) is an essential gene for tumour cells that express ISGs (5, 44). Even  
457 more importantly, ADAR has been shown to be involved in resistance to ICB therapy and  
458 irradiation in preclinical models (4). The molecular basis of these observations is to the  
459 excessive accumulation of dsRNA induced by the absence of ADAR and the subsequent  
460 activation of the sensors for this innate ligand, mainly PKR and the axis DDX58/IFIH1,  
461 leading to cell death and tumour inflammation (4, 5, 44). As we found ADAR to be highly  
462 modified in the KO cells treated with IFN, we decided to check if in our cellular model  
463 ADAR is also essential upon activation of the IFN pathway. To do so, we silenced ADAR  
464 with specific siRNA sequences in HAP1 WT cells and we subsequently treated them with  
465 IFN. In a similar fashion to USP18 depletion, ADAR genetic inactivation also sensitises  
466 HAP1 cells to IFN (Fig. 4A). In addition to its effects on cell growth, we evaluated the  
467 activation of the dsRNA sensor PKR, measured by phosphorylation at threonine 446, in  
468 WT and USP18 KO cells treated with IFN for 0, 6, 24 and 48 hours. Both, ADAR and  
469 PKR are ISGylated upon IFN treatment but only in the USP18 KO cells (Fig. 4B).  
470 ISGylation of PKR fits with its markedly higher phosphorylation in the KO cells compared  
471 with a relatively modest activation in the WT cells because ISGylation of PKR (although  
472 on different residues) has been previously reported to activate PKR (42). We identified 7  
473 lysine residues in the sequence of ADAR that are potentially ISGylated (K433, K637,  
474 K763, K781, K798, K895, and K996; Fig. 4C). When highlighting these residues in the  
475 structure of the deaminase domain of ADAR2 bound to RNA, three of them seem to  
476 directly contribute to the binding of the enzyme to RNA (K637, K781, and K996; Fig. 4D).  
477 Finally, we measured the levels of the innate ligand dsRNA in our cells using specific  
478 antibodies against dsRNA by immunofluorescence as an indication of ADAR activity.

ADAR enzymes are responsible for binding to double-stranded RNA (dsRNA) and converting adenosine (A) to inosine (I) by deamination, thus reducing the intracellular levels of dsRNA. The results shown in Fig. 4E and 4F illustrate the accumulation of dsRNA in a time-dependent manner only in the USP18 KO cells treated with IFN for 0, 24 and 48 hours. This accumulation matches well with the ISGylation levels of ADAR p150 seen in Fig. 4B and points at USP18 and ISG15 as key regulators of ADAR deaminase activity.

#### **USP18 regulates MHC class I antigen presentation, PD-L1 expression and stimulation of a T cell functional response**

In the USP18-dependent ISGylome and proteome of cancer cells treated with type I IFN, we observed ISGylated components of the antigen presentation pathway (Fig. 2F, 2G, and 3E). To test whether USP18 modulates antigen presentation and T cell stimulation, we pulsed the HLA-A2 positive HAP1 cell line (WT and USP18 KO; with and without pre-treatment with IFN for 24 hours) with different concentrations of the HLA-A2-restricted Melan-A<sub>26-35</sub> peptide and then co-cultured them with Melan-A specific CTL for 18 hours (37, 45).

Peptide-pulsed WT or USP18 KO HAP1 cells (+/- type I IFN pre-treatment) stimulated phenotypic activation of T cells (as assessed by upregulation of the activation markers CD25 and CD137) with equal efficiency (Fig.5A). However, both with and without IFN pre-treatment, the USP18 KO cells triggered a more robust functional response by the T cells, as evidenced by greater T cell production of IFN $\gamma$  following peptide recognition (Fig. 5B). Since the strength of the activating stimulus received by T cells determines the nature of their response, with phenotypic activation and production of chemokines such as MIP1 $\beta$  being more readily triggered than production of cytokines such as IFN $\gamma$  (46), this suggests that USP18-deficient tumour cells exhibit superior antigenicity. Non-peptide-pulsed HAP1 USP18 KO cells expressed a similar level of HLA-A2 to the

parental cells and HLA-A2 was equivalently upregulated on both following exposure to type 1 IFN (Fig. 5C, top left histogram plot). HLA-A2 was further upregulated on both WT and KO cells after pulsing with the Melan-A<sub>26-35</sub> peptide and co-culture with T cells, likely in response to IFN $\gamma$  secreted by the T cells (Fig. 5C; top right and lower histogram plots). However, a proportion of the peptide-pulsed cells exhibited downregulation of HLA-A2 to levels below those expressed on non-peptide-pulsed cells following co-culture with T cells, potentially because of HLA-A2 internalisation and/or degradation (Fig. 5C; top right and lower histogram plots). Notably, high levels of HLA-A2 expression were retained on a greater proportion of the USP18 KO cells than their WT counterparts (Fig. 5C; bottom graph), putatively contributing to their greater antigenicity.

Strikingly, we observed a strong upregulation of PD-L1 on both tumour cells (Fig. 5D) and T cells when USP18 was absent (Fig. 5E). This effect was antigen dependent, although the KO cells pre-treated with type I IFN presented a high basal expression of PD-L1 in the absence of peptide. PD-L1 protein expression in tumours has been described as a potential predictive biomarker for sensitivity to immune checkpoint blockade (ICB) with PD1/PD-L1 inhibitors (47). Also, we observed an upregulation of PD-L1 levels on the T cells when co-cultured with USP18 KO cancer cells, regardless of treatment. In contrast, very little upregulation of PD-L1 was noted on T cells stimulated with WT cells (+/- IFN), after addition of peptide (Fig. 5E). PD-L1 is expressed on activated T cells and is required for T cell conditioning and dendritic cell maturation (48). However, its expression on T cells has been mostly linked to inhibition of their responses (49). Other studies indicates that expression of PD-L1 on CD8<sup>+</sup> and CD4<sup>+</sup> T cells correlates with patient response to ICB, suggesting PD-L1 expression in CD8<sup>+</sup> T cells as a prognostic marker in melanoma (9, 50).

## **USP18 deficiency sensitises cancer cells to radiation therapy (RT)**

530 Efficacy of local radiotherapy (RT) has been linked to the ability of the irradiated cells to  
531 repair lethal DNA damage but also to the induction of T cell-dependent cell killing. This  
532 immune attack has been linked to the induction of the type I IFN response after tumour  
533 RT (10) and also seems to be ADAR-dependent (4). As shown above, USP18-deficient  
534 HAP1 cells displayed greater cellular death following activation of IFN signalling by  
535 exposure to type I IFN in tissue culture. Thus, we hypothesized that loss of USP18 in  
536 cancer cell could also augment their sensitivity to ionizing radiation. Indeed, USP18 KO  
537 cells exhibited a significantly lower clonogenic survival rate after radiation in tissue  
538 culture compared with WT (representative images in Fig. 6A and summary in Fig. 6B). In  
539 addition, the average colony diameter of USP18 KO cells was smaller than that of WT  
540 (Fig. 6C) indicating that USP18 deficiency also results in greater growth delay after  
541 exposure to ionizing radiation. Consistently, following a single dose of 5Gy irradiation,  
542 the cell number ratio of WT over USP18 KO cell increased over time (Fig. 6D).

## 543 **Discussion**

544 This study provides a comprehensive profile of the USP18-regulated human  
545 endogenous ISGylome at a site-specific resolution. USP18 is the predominant  
546 deISGylating enzyme that processes ISG15 *in vivo* and, like ISG15, its expression is  
547 induced in the presence of agonists of the interferon pathway. USP18-deficient cells are  
548 sensitive to IFN treatment and strongly accumulate ISGylated proteins without noticeable  
549 effects on ubiquitylation or NEDDylation. This effect seems to be dependent on the  
550 catalytic activity of USP18, contradicting some previously reported studies on mice and  
551 humans. Notably, in this study, we used specific ISG15 activity-based probes to  
552 demonstrate that the catalytically inactive mutant enzyme (C64A/C65A) is actually  
553 inactive. This is particularly important in the case of USP18 since there is an additional  
554 cysteine (C65) adjacent to the catalytic cysteine (C64). When performing activity assays,  
555 we found that single mutants C64S and C64R were still active (data not shown). Here,  
556 we were able to identify 2341 GlyGly sites and 476 enriched modified proteins that, after

557 exhaustive validation using orthogonal techniques, we were confident to label them as  
558 ISGylated proteins and map their modified sites. When comparing our data with previous  
559 ISGylome studies, 537 new ISGylated human proteins were identified (Fig. S4B). Hence,  
560 this study expands considerably the human, USP18-dependent, ISGylome, suggesting  
561 novel regulatory cellular functions by ISGylation. A cross-comparison between the  
562 GlyGly peptidome data and the matching proteome further confirmed that ISGylation is  
563 not involved in protein degradation, but rather stabilisation, perhaps through co-  
564 translational modification (51). In addition, the overall expression level of many of the  
565 ISGylated proteins does not change, reinforcing the role of ISG15 as a PTM modulating  
566 enzymatic activities (42).

567 Pathway analysis could identify some significantly enriched biological processes  
568 modulated by USP18-dependent ISGylation such as dsRNA binding, innate immune  
569 response, defence to virus, translation and glycolysis/gluconeogenesis. Many of these  
570 proteins are ISGs, and a number of them are part of a signature of genes that are  
571 upregulated in a subset of tumour cells, independent of immune infiltration (5). ISG-  
572 positive cancer cells are sensitive to ADAR loss, another ISG with deaminase activity,  
573 controlling the levels of dsRNA, an innate ligand (5, 44). We identified USP18-dependent  
574 ISG15ylation in seven lysine residues for ADAR (K433, K637, K763, K781, K798, K895,  
575 and K996), localised within the dsRNA binding (dsRBD) and deaminase domains (DD),  
576 which may potentially affect both enzymatic activity and substrate binding affinity. ADAR  
577 has been recently described as a major factor for resistance to immunotherapy and  
578 radiotherapy (4). In our model, ADAR gene silencing using siRNA sequences sensitises  
579 cancer cells to IFN stimulation in a similar fashion as USP18 does. We could detect  
580 ISGylated ADAR by immunoblotting in USP18-deficient cells after 24 hours treatment  
581 with IFN, and this time point matched the time when the growth of the cells started to be  
582 inhibited by this cytokine. The described effects of ADAR loss in overcoming  
583 immunotherapy and radiotherapy have been linked to its ability to reduce the levels of

584 innate ligand dsRNA and subsequent inhibition of the dsRNA sensors PKR, and  
585 MDA5/RIG-I, involved in growth inhibition and tumour inflammation, respectively (4, 5,  
586 44). ISGylation of PKR has been reported to activate its activity, and we could also see  
587 ISGylation and activation of PKR in the USP18 KO cells treated with IFN. Our data,  
588 therefore, suggested that USP18-dependent ISGylation of ADAR was inhibiting its  
589 activities, inducing the accumulation of dsRNA, resulting in further activation of PKR.  
590 Immunofluorescence analysis using specific dsRNA antibodies showed a significant and  
591 time-dependent accumulation of dsRNA in the USP18 KO cells after IFN treatment,  
592 indicating that USP18-dependent ISGylation under these conditions could inhibit ADAR  
593 activity.

594 In addition to ADAR, PKR, RIG-I, and MDA5, we found other proteins involved in antigen  
595 presentation and resistance to immunotherapy, such as TAP1, GBP1, STAT1, IFIT1,  
596 PSMB10, PSMB9, GBP2, MAGE and PARP14 (41), also regulated by USP18-  
597 dependent ISGylation. Many of these genes are part of processing MHC class I  
598 antigens, suggesting that the USP18 KO cells could possibly be more antigenic. Indeed,  
599 our results confirmed that USP18 KO cells had an enhanced ability to stimulate IFN $\gamma$   
600 secretion by Melan-A antigen-specific T cells, which was associated with elevated HLA-  
601 A2 expression levels. Interestingly, PD-L1 levels, a prognostic factor for ICB therapy  
602 when using PD1 inhibitors, were also higher in USP18 KO as compared to WT cells, and  
603 PD-L1 was also upregulated on the T cells following interaction with these cells. This is  
604 noteworthy as other studies have linked the expression of PD-L1 on CD8<sup>+</sup> and CD4<sup>+</sup> T  
605 cells with patient response to ICB, suggesting PD-L1 expression in CD8<sup>+</sup> T cells as a  
606 prognostic marker in melanoma (9, 50). As the innate immune response is activated by  
607 radiotherapy (10) and ADAR recently described as an important factor in resistance to  
608 RT (4), we decided to perform a second round of functional experiments consisting of  
609 irradiating our cancer cells and evaluating viability and clonogenicity after RT. The

610 results clearly suggest that USP18 deficiency sensitises tumour cells to RT in a dose-  
611 dependent manner, most likely by interfering with end-stage IFN signalling.

612 Directing the immune system against tumours, also known as cancer immunotherapy, is  
613 supplementing or replacing more conventional forms of therapy as the first line of  
614 treatment for many tumour types due to striking curative effects in a subset of the treated  
615 patients. However, resistance mechanisms prevent this therapy from being 100%  
616 effective. The innate immune response has been described as one of the main  
617 resistance mechanisms against resistance to ICB and the discovery of factors involved  
618 in reactivation of the innate response, such as ADAR, has been a priority for the cancer  
619 research community. So far, inhibition of ADAR has been unfruitful. Our data suggest  
620 that USP18 inhibition represents a novel strategy to block ADAR functions, to activate  
621 the immunoproteasome/antigen presentation machinery and innate ligand sensors. As a  
622 consequence, this may help to overcome resistance to immunotherapy and RT,  
623 potentially turning 'cold' tumours into 'hot' tumours."

#### 624 **Additional Information:**

625 - **Acknowledgments:** We would like to thank the TDI MS Laboratory/Discovery  
626 Proteomics Facility for their technical support and Sebastian Nijman for providing the  
627 USP18-deficient HAP1 cells. We would also thank Paul Wes and his team at Pfizer-CTI  
628 (Centers for Therapeutic Innovation; New York) for their helpful discussions. A preprint of  
629 this manuscript is available on the open access repository bioRxiv (52).

630 - **Authors' contribution:** APF, EA, NJ, TJ, KH, RM, PB, VC, and BMK directed  
631 this study. Most experiments were devised by APF and BMK, and carried out by APF.  
632 MS helped, supervised, and assisted with the T Cell experiments. TP helped, supervised  
633 and assisted with the T Cell experiments. JC helped, supervised and assisted with the  
634 radiation therapy experiments. GV performed immunoblots and helped with the  
635 published ISGylome comparison. HG carried out cell viability experiments. CSO  
636 performed immunofluorescence experiments. AD generated the catalytically inactive

USP18 mutant. HCS assisted with the ISG-PA activity-based probe synthesis. HJP, BP, and AC helped to establish the ISG15 immunoprecipitation method. LDS and PS helped with ADAR structural analyses. CGL provided support with the T cell experiments. APF wrote the manuscript with the help of BMK, PB, and TP. All authors commented on the text.

- **Ethics approval and consent to participate:** HAP1 cells (WT and KO) are a kind gift from the laboratory of Sebastian Nijman and the HCT116 cell line was purchased from ATCC (ATCC-CCL-247).

- **Consent for publication:** Not applicable.

- **Data availability:** The mass spectrometry proteomics data have been deposited to the ProteomeXchange Consortium via the PRIDE (53) partner repository with the data set identifier PXD018299.

- **Conflict of Interest:** No potential conflicts of interest were disclosed.

- **Funding:** Work in the BMK lab was funded by FORMA Therapeutics, Pfizer Inc., by an EPSRC grant EP/N034295/1 and by the Chinese Academy of Medical Sciences (CAMS) Innovation Fund for Medical Science (CIFMS), China (grant number: 2018-I2M-2-002).

## References

1. Zaretsky JM, Garcia-Diaz A, Shin DS, Escuin-Ordinas H, Hugo W, Hu-Lieskovan S, et al. Mutations Associated with Acquired Resistance to PD-1 Blockade in Melanoma. *N Engl J Med*. 2016;375(9):819-29.
2. Michot JM, Bigenwald C, Champiat S, Collins M, Carbonnel F, Postel-Vinay S, et al. Immune-related adverse events with immune checkpoint blockade: a comprehensive review. *Eur J Cancer*. 2016;54:139-48.
3. Shin DS, Zaretsky JM, Escuin-Ordinas H, Garcia-Diaz A, Hu-Lieskovan S, Kalbasi A, et al. Primary Resistance to PD-1 Blockade Mediated by JAK1/2 Mutations. *Cancer Discov*. 2017;7(2):188-201.
4. Ishizuka JJ, Manguso RT, Cheruiyot CK, Bi K, Panda A, Iracheta-Vellve A, et al. Loss of ADAR1 in tumours overcomes resistance to immune checkpoint blockade. *Nature*. 2019;565(7737):43-8.
5. Liu H, Golji J, Brodeur LK, Chung FS, Chen JT, deBeaumont RS, et al. Tumor-derived IFN triggers chronic pathway agonism and sensitivity to ADAR loss. *Nat Med*. 2019;25(1):95-102.
6. Yoshihama S, Roszik J, Downs I, Meissner TB, Vijayan S, Chapuy B, et al. NLRC5/MHC class I transactivator is a target for immune evasion in cancer. *Proceedings of the National Academy of Sciences of the United States of America*. 2016;113(21):5999-6004.

- 672 7. Sade-Feldman M, Jiao YJ, Chen JH, Rooney MS, Barzily-Rokni M, Eliane JP, et al.  
673 Resistance to checkpoint blockade therapy through inactivation of antigen presentation. *Nat*  
674 *Commun.* 2017;8(1):1136.
- 675 8. Li K, Qu S, Chen X, Wu Q, Shi M. Promising Targets for Cancer Immunotherapy: TLRs,  
676 RLRs, and STING-Mediated Innate Immune Pathways. *International journal of molecular*  
677 *sciences.* 2017;18(2).
- 678 9. Jacquelot N, Roberti MP, Enot DP, Rusakiewicz S, Ternes N, Jegou S, et al. Predictors of  
679 responses to immune checkpoint blockade in advanced melanoma. *Nat Commun.*  
680 2017;8(1):592.
- 681 10. McLaughlin M, Patin EC, Pedersen M, Wilkins A, Dillon MT, Melcher AA, et al.  
682 Inflammatory microenvironment remodelling by tumour cells after radiotherapy. *Nat Rev*  
683 *Cancer.* 2020;20(4):203-17.
- 684 11. Havens CG, Bjorklund C, Kang J, Ortiz M, Fontanillo C, Amatangelo M, et al. IMiDs®  
685 Immunomodulatory Agents Regulate Interferon-Stimulated Genes through Cereblon-Mediated  
686 Aiolos Destruction in Multiple Myeloma (MM) Cells: Identification of a Novel Mechanism of  
687 Action and Pathway for Resistance. *Blood* 2014.
- 688 12. Catic A, Fiebiger E, Korb GA, Blom D, Galardy PJ, Ploegh HL. Screen for ISG15-  
689 crossreactive deubiquitinases. *PLoS One.* 2007;2(7):e679.
- 690 13. Ye Y, Akutsu M, Reyes-Turcu F, Enchev RI, Wilkinson KD, Komander D. Polyubiquitin  
691 binding and cross-reactivity in the USP domain deubiquitinase USP21. *EMBO reports.*  
692 2011;12(4):350-7.
- 693 14. Basters A, Geurink PP, Rocker A, Witting KF, Tadayon R, Hess S, et al. Structural basis of  
694 the specificity of USP18 toward ISG15. *Nature structural & molecular biology.* 2017;24(3):270-8.
- 695 15. Ketscher L, Hanns R, Morales DJ, Basters A, Guerra S, Goldmann T, et al. Selective  
696 inactivation of USP18 isopeptidase activity in vivo enhances ISG15 conjugation and viral  
697 resistance. *Proc Natl Acad Sci U S A.* 2015;112(5):1577-82.
- 698 16. Villarroya-Beltri C, Guerra S, Sanchez-Madrid F. ISGylation - a key to lock the cell gates  
699 for preventing the spread of threats. *J Cell Sci.* 2017;130(18):2961-9.
- 700 17. Jimenez Fernandez D, Hess S, Knobloch KP. Strategies to Target ISG15 and USP18  
701 Toward Therapeutic Applications. *Front Chem.* 2019;7:923.
- 702 18. Sarasin-Filipowicz M, Wang X, Yan M, Duong FH, Poli V, Hilton DJ, et al. Alpha interferon  
703 induces long-lasting refractoriness of JAK-STAT signaling in the mouse liver through induction of  
704 USP18/UBP43. *Mol Cell Biol.* 2009;29(17):4841-51.
- 705 19. Malakhova OA, Yan M, Malakhov MP, Yuan Y, Ritchie KJ, Kim KI, et al. Protein ISGylation  
706 modulates the JAK-STAT signaling pathway. *Genes & development.* 2003;17(4):455-60.
- 707 20. Knobloch KP, Utermohlen O, Kisser A, Prinz M, Horak I. Reexamination of the role of  
708 ubiquitin-like modifier ISG15 in the phenotype of UBP43-deficient mice. *Mol Cell Biol.*  
709 2005;25(24):11030-4.
- 710 21. Zhang X, Bogunovic D, Payelle-Brogard B, Francois-Newton V, Speer SD, Yuan C, et al.  
711 Human intracellular ISG15 prevents interferon-alpha/beta over-amplification and auto-  
712 inflammation. *Nature.* 2015;517(7532):89-93.
- 713 22. Tokarz S, Berset C, La Rue J, Friedman K, Nakayama K, Nakayama K, et al. The ISG15  
714 isopeptidase UBP43 is regulated by proteolysis via the SCFSkp2 ubiquitin ligase. *J Biol Chem.*  
715 2004;279(45):46424-30.
- 716 23. Bogunovic D, Byun M, Durfee LA, Abhyankar A, Sanal O, Mansouri D, et al.  
717 Mycobacterial disease and impaired IFN-gamma immunity in humans with inherited ISG15  
718 deficiency. *Science.* 2012;337(6102):1684-8.
- 719 24. Sapmaz A, Berlin I, Bos E, Wijdeven RH, Janssen H, Konietzny R, et al. USP32 regulates  
720 late endosomal transport and recycling through deubiquitylation of Rab7. *Nature*  
721 *communications.* 2019;10(1):1454.

- 722 25. Honke N, Shaabani N, Zhang DE, Hardt C, Lang KS. Multiple functions of USP18. *Cell*  
723 *death & disease*. 2016;7(11):e2444.
- 724 26. Mustachio LM, Lu Y, Kawakami M, Roszik J, Freemantle SJ, Liu X, et al. Evidence for the  
725 ISG15-Specific Deubiquitinase USP18 as an Antineoplastic Target. *Cancer research*.  
726 2018;78(3):587-92.
- 727 27. Meuwissen ME, Schot R, Buta S, Oudesluijs G, Tinschert S, Speer SD, et al. Human USP18  
728 deficiency underlies type 1 interferonopathy leading to severe pseudo-TORCH syndrome. *J Exp*  
729 *Med*. 2016;213(7):1163-74.
- 730 28. Potu H, Sgorbissa A, Brancolini C. Identification of USP18 as an important regulator of  
731 the susceptibility to IFN-alpha and drug-induced apoptosis. *Cancer research*. 2010;70(2):655-65.
- 732 29. Gaston J, Cheradame L, Yvonnet V, Deas O, Poupon MF, Judde JG, et al. Intracellular  
733 STING inactivation sensitizes breast cancer cells to genotoxic agents. *Oncotarget*.  
734 2016;7(47):77205-24.
- 735 30. Radoshevich L, Impens F, Ribet D, Quereda JJ, Nam Tham T, Nahori MA, et al. ISG15  
736 counteracts *Listeria monocytogenes* infection. *Elife*. 2015;4.
- 737 31. Giannakopoulos NV, Luo JK, Papov V, Zou W, Lenschow DJ, Jacobs BS, et al. Proteomic  
738 identification of proteins conjugated to ISG15 in mouse and human cells. *Biochem Biophys Res*  
739 *Commun*. 2005;336(2):496-506.
- 740 32. Durfee LA, Huibregtse JM. Identification and Validation of ISG15 Target Proteins. *Subcell*  
741 *Biochem*. 2010;54:228-37.
- 742 33. Zhao C, Denison C, Huibregtse JM, Gygi S, Krug RM. Human ISG15 conjugation targets  
743 both IFN-induced and constitutively expressed proteins functioning in diverse cellular pathways.  
744 *Proc Natl Acad Sci U S A*. 2005;102(29):10200-5.
- 745 34. Takeuchi T, Inoue S, Yokosawa H. Identification and Herc5-mediated ISGylation of novel  
746 target proteins. *Biochem Biophys Res Commun*. 2006;348(2):473-7.
- 747 35. Wong JJ, Pung YF, Sze NS, Chin KC. HERC5 is an IFN-induced HECT-type E3 protein ligase  
748 that mediates type I IFN-induced ISGylation of protein targets. *Proc Natl Acad Sci U S A*.  
749 2006;103(28):10735-40.
- 750 36. Pinto A, Mace Y, Drouet F, Bony E, Boidot R, Draoui N, et al. A new ER-specific  
751 photosensitizer unravels (1)O<sub>2</sub>-driven protein oxidation and inhibition of deubiquitinases as a  
752 generic mechanism for cancer PDT. *Oncogene*. 2016;35(30):3976-85.
- 753 37. Salio M, Shepherd D, Dunbar PR, Palmowski M, Murphy K, Wu L, et al. Mature dendritic  
754 cells prime functionally superior melan-A-specific CD8<sup>+</sup> lymphocytes as compared with  
755 nonprofessional APC. *J Immunol*. 2001;167(3):1188-97.
- 756 38. Pinto-Fernandez A, Davis S, Schofield AB, Scott HC, Zhang P, Salah E, et al.  
757 Comprehensive Landscape of Active Deubiquitinating Enzymes Profiled by Advanced  
758 Chemoproteomics. *Front Chem*. 2019;7:592.
- 759 39. Arimoto KI, Lochte S, Stoner SA, Burkart C, Zhang Y, Miyauchi S, et al. STAT2 is an  
760 essential adaptor in USP18-mediated suppression of type I interferon signaling. *Nat Struct Mol*  
761 *Biol*. 2017;24(3):279-89.
- 762 40. Zhang Y, Thery F, Wu NC, Luhmann EK, Dussurget O, Foecke M, et al. The in vivo  
763 ISGylome links ISG15 to metabolic pathways and autophagy upon *Listeria monocytogenes*  
764 infection. *Nat Commun*. 2019;10(1):5383.
- 765 41. Harel M, Ortenberg R, Varanasi SK, Mangalhara KC, Mardamshina M, Markovits E, et al.  
766 Proteomics of Melanoma Response to Immunotherapy Reveals Mitochondrial Dependence. *Cell*.  
767 2019;179(1):236-50 e18.
- 768 42. Okumura F, Okumura AJ, Uematsu K, Hatakeyama S, Zhang DE, Kamura T. Activation of  
769 double-stranded RNA-activated protein kinase (PKR) by interferon-stimulated gene 15 (ISG15)  
770 modification down-regulates protein translation. *J Biol Chem*. 2013;288(4):2839-47.

771 43. Desai SD, Haas AL, Wood LM, Tsai YC, Pestka S, Rubin EH, et al. Elevated expression of  
772 ISG15 in tumor cells interferes with the ubiquitin/26S proteasome pathway. *Cancer Res.*  
773 2006;66(2):921-8.

774 44. Gannon HS, Zou T, Kiessling MK, Gao GF, Cai D, Choi PS, et al. Identification of ADAR1  
775 adenosine deaminase dependency in a subset of cancer cells. *Nat Commun.* 2018;9(1):5450.

776 45. Mezzadra R, de Bruijn M, Jae LT, Gomez-Eerland R, Duursma A, Scheeren FA, et al.  
777 SLFN11 can sensitize tumor cells towards IFN-gamma-mediated T cell killing. *PLoS One.*  
778 2019;14(2):e0212053.

779 46. Almeida JR, Sauce D, Price DA, Papagno L, Shin SY, Moris A, et al. Antigen sensitivity is a  
780 major determinant of CD8+ T-cell polyfunctionality and HIV-suppressive activity. *Blood.*  
781 2009;113(25):6351-60.

782 47. Kalbasi A, Ribas A. Tumour-intrinsic resistance to immune checkpoint blockade. *Nat Rev*  
783 *Immunol.* 2020;20(1):25-39.

784 48. Talay O, Shen CH, Chen L, Chen J. B7-H1 (PD-L1) on T cells is required for T-cell-mediated  
785 conditioning of dendritic cell maturation. *Proc Natl Acad Sci U S A.* 2009;106(8):2741-6.

786 49. Diskin B, Adam S, Cassini MF, Sanchez G, Liria M, Aykut B, et al. PD-L1 engagement on T  
787 cells promotes self-tolerance and suppression of neighboring macrophages and effector T cells  
788 in cancer. *Nat Immunol.* 2020.

789 50. Jacquelot N, Zitvogel L, Eggermont AM. Reply to 'Challenging PD-L1 expressing cytotoxic  
790 T cells as a predictor for response to immunotherapy in melanoma'. *Nat Commun.*  
791 2018;9(1):2922.

792 51. Durfee LA, Lyon N, Seo K, Huibregtse JM. The ISG15 conjugation system broadly targets  
793 newly synthesized proteins: implications for the antiviral function of ISG15. *Mol Cell.*  
794 2010;38(5):722-32.

795 52. Pinto-Fernandez A, Salio M, Partridge T, Chen J, Vere G, Greenwood H, et al. Deep  
796 analysis of the USP18-dependent ISGylome and proteome unveils important roles for USP18 in  
797 tumour cell antigenicity and radiosensitivity. 2020:2020.03.31.005629.

798 53. Perez-Riverol Y, Csordas A, Bai J, Bernal-Llinares M, Hewapathirana S, Kundu DJ, et al.  
799 The PRIDE database and related tools and resources in 2019: improving support for  
800 quantification data. *Nucleic Acids Res.* 2019;47(D1):D442-D50.

801

## 802 **Figure Legends**

### 803 **Figure 1: USP18 alters protein ISGylation and cell viability in presence of IFN. A)**

804 Depiction of the roles of USP18. USP18 is an interferon-stimulated gene (ISG) that acts  
805 as a negative regulator of the type I interferon (IFN) signalling pathway and removes  
806 ISG15, another ISG structurally similar to a dimer of ubiquitin, from modified proteins. **B)**  
807 HAP1 CML-derived wild-type (WT) and USP18 knockout cells (KO) growth is  
808 comparable. **C)** The growth of HAP1 cells deficient for USP18 is inhibited by type I IFN  
809 treatment. **D)** Immunoblot showing cleavage of the pro-apoptotic marker cPARP in HAP1  
810 USP18<sup>-/-</sup> cells after 48 h. treatment with IFN. **E)** Immunoblot showing induction of

USP18 after 24 h. and 48 h. of treatment with IFN in WT cells and accumulation of conjugated ISG15 in USP18-deficient cells in the same conditions. **F)** Stable re-expression of USP18 WT, but not of a catalytically inactive mutant USP18 C64R/C65R, in USP18-deficient cells rescue them from the growth-inhibitory effects of IFN. **G)** Immunoblot of cell extracts from USP18 KO cells expressing USP18 WT and USP18 C64R/C65R. Ectopic expression of WT but not catalytically inactive USP18 prevents the accumulation of ISGylated proteins upon IF treatment (top panel). ISG15 propargylamide (ISG15-PA) activity-based probe (ABP) labels only USP18 WT, whilst it is unreactive towards the catalytically inactive mutant (middle panel). GAPDH was used as a loading control in all the immunoblots.

**Figure 2: USP18 is the major cellular de-ISGylase.** **A)** Workflow for analysis of GlyGly-modified peptides. **B)** Comparative table of the C-terminal motifs of the different ubiquitin-like proteins. ISG15, Ubiquitin, and NEDD8 leave a unique GlyGly motif (in green) after trypsin digestion of modified proteins. **C)** Ubiquitin-conjugated and **D)** NEDD8-conjugated proteins do not increase after stimulation with type I interferon (IFN) in USP18 KO cells. **E)** ISG15 modification is accumulated in the same conditions as in **C).** **F)** Comparative volcano plot of the GlyGly modified peptides in HAP1 WT and USP18 KO cells treated with IFN for 48 h showing a strong and significant USP18-dependent upregulation of GlyGly-modified peptides in the KO cells treated with IFN for 48 h. In red are shown the upregulated peptides in the KO cells, in green the upregulated peptides in WT cells, and in blue the modified peptides from an ISG-cancer signature (5) (the statistical cut-off values used for all the proteomic analyses performed in this study are FDR: 0.01 and s0: 0.1). Pathway enrichment analysis showed the upregulated peptides in the USP18 KO cells come from proteins involved in the indicated biological processes. **G)** Scatter plot of the cross-comparative analysis of ISGylome and proteome in the same conditions as **F).** In red are shown the upregulated ISGylated proteins in the KO cells, in green the upregulated modified proteins in WT cells, and in blue the modified proteins from an ISG-cancer signature (5).

**Figure 3: USP18-deletion exacerbates the cellular ISGylated protein network.** **A)** Immunoblot using specific antibodies against the indicated proteins showing additional ISGylation of these proteins in the HAP1 USP18 KO cells treated with IFN. **B)** HAP1 USP18 KO cells were transfected with siRNA sequences targeting ISG15 and ADAR and treated with IFN for the indicated times. After ISG15 silencing, modified ADAR (ADAR1 (p150)-ISG15; lower panel) is no longer visible by immunoblot. **C)** HAP1 WT and USP18 KO cells were treated with IFN for the indicated times, lysed and subjected to immunoprecipitation (IP) with ISG15 antibodies. Enriched ISGylated proteins were present in eluates from the USP18 KO cells (top panel) but there was no enrichment for ubiquitinated proteins (lower panel). **D)** Immunoblot of the same eluates in C) against the indicated proteins showing enrichment for ISGylated species. **E)** Volcano plot of comparative proteomic analysis of the IP eluates in C) and D). Pathways enriched are shown. Comparative scatter plot **F)** of the GlyGly peptide IP and the ISG15 IP, performed in the same experimental conditions showing a strong overlap between the two data sets and strong enrichment of members of the ISG cancer gene signature (5) and factors up-regulated in PD1-responders (41).

**Figure 4: USP18-dependent ISGylation of ADAR leads to enzymatic activity inhibition and dsRNA accumulation.** ADAR knockdown using siRNA renders HAP1 WT sensitive to growth inhibition by type I IFN as shown by the growth curves in **A)**. **B)** Immunoblots of a time-course experiment showing an increase in modified ADAR and PKR and activation of PKR (phosphorylated PKR in Thr 446) USP18-deficient cells treated with IFN for the indicated times. **C)** A plot of the ADAR GlyGly-modified lysines and their ion intensities measured by MS. **D)** dsRNA bound ADAR2 deaminase domain structure (PDB code 5ED2). Lysine residues corresponding to the ADAR1 GlyGly sites are represented with sticks. The  $Zn^{2+}$  cation is represented as a grey sphere (top panel). Table showing the ADAR1 potential GlyGly sites indicating their domain location and their contribution to RNA binding. A score of 1 indicates the highest contribution and 3 the lowest and away from the RNA binding pocket. DD = deaminase domain. dsRBD =

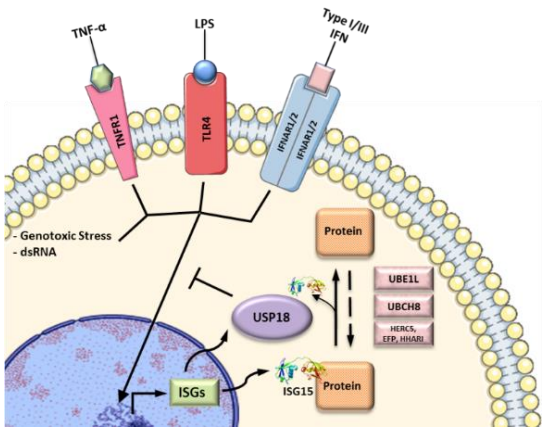
dsRNA binding domain (lower panel). **E) and F)** Analysis of the dsRNA levels after IFN treatment in WT and KO cells by immunofluorescence using specific antibodies (n=6 per condition).

**Figure 5. USP18 regulates major histocompatibility complex class I (MHC-I) antigen presentation, PD-L1 expression and stimulation of a T cell response.** Wild-type or USP18-deficient HAP1 cells were pre-treated with or without IFN- $\alpha$ , then pulsed with Melan-A<sub>26-35</sub> peptide at the indicated concentrations and co-cultured with Melan-A-specific T cells. **A)** Upregulation of activation markers on T cells was assessed by flow cytometry. Dotplots show representative examples of CD25 and CD137 expression on live CD2<sup>+</sup> cells (T cells) following co-culture with the indicated peptide-pulsed HAP1 cells and the proportion of T cells expressing both CD25 and CD137 is plotted below. **B)** T cell release of IFN $\gamma$  into HAP1-T cell co-culture supernatants was measured by ELISA. Bars show mean values from 3 replicates and for the statistical analysis, we applied two-way ANOVA tests including multiple comparison testing via the Dunnett method available through the GraphPad Prism software. P value style is GraphPad: NS, P = 0.1234, \*P = 0.0332, \*\*P = 0.0021, \*\*\*P = 0.0002, \*\*\*\*P < 0.0001. Expression of **C)** HLA-A2 and **D)** PD-L1 on HAP1 cells following co-culture with T cells was measured by flow cytometry. Histogram plots of the data are shown above, and the plots below show the percentage of cells C) expressing high levels of HLA-A2 (defined as greater than those expressed on non-peptide-pulsed cells not pre-treated with type 1 IFN and D) expressing PD-L1. **E)** PD-L1 expression on T cells following co-culture with the indicated HAP1 cells. Representative histogram plots are shown above, and the geometric mean fluorescence intensity (gMFI) of PD-L1 expression on T cells from each co-culture condition is plotted below. The results shown in this figure are representative of data from 1 of 3 experiments and the FACS shows information of three replicates pooled into one. Event counts on histogram plots have been normalised to unit area to enable comparison between samples.

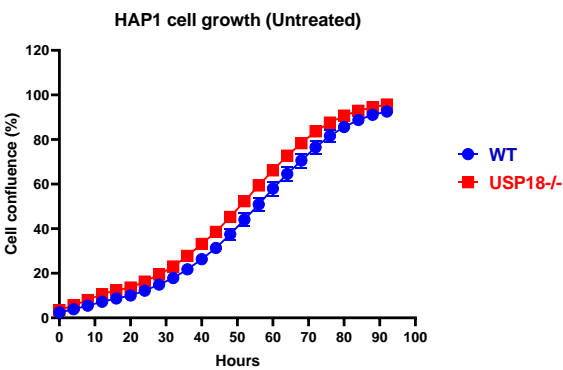
894 **Figure 6: Deletion of USP18 increases cellular radiosensitivity (IR): A)**  
895 Representative images of clonogenic assay with HAP1 WT cells (left column) and HAP1  
896 USP18KO (right column). The IR doses and seeding cell numbers were indicated. **B)**  
897 Quantitation of data from the clonogenic assay measured as survival fraction in the  
898 same conditions as in a). n = 3 biological repeats. **C)** The diameter of the counted  
899 colonies in a) and b). n = 3. **D)** Cell number ratio of WT vs USP18 -/- HAP1 cells at  
900 indicated time points after a single dose of 5Gy IR. Data represent mean  $\pm$  SD.  
901 Comparison of two means was performed by the one-way ANOVA (\* P < 0.05, \*\* P <  
902 0.01, \*\*\* P < 0.001).

Figure 1

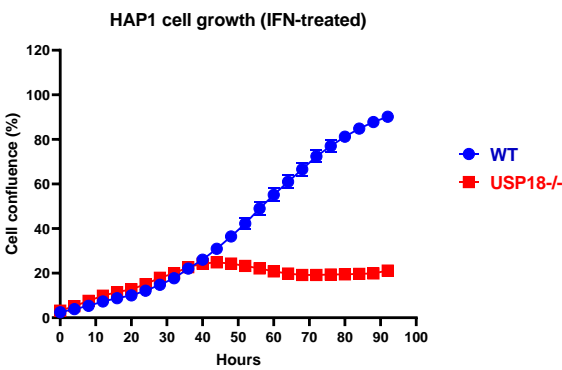
A



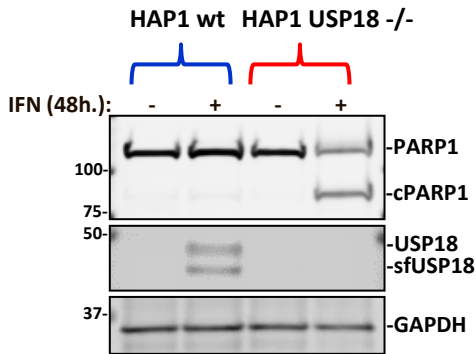
B



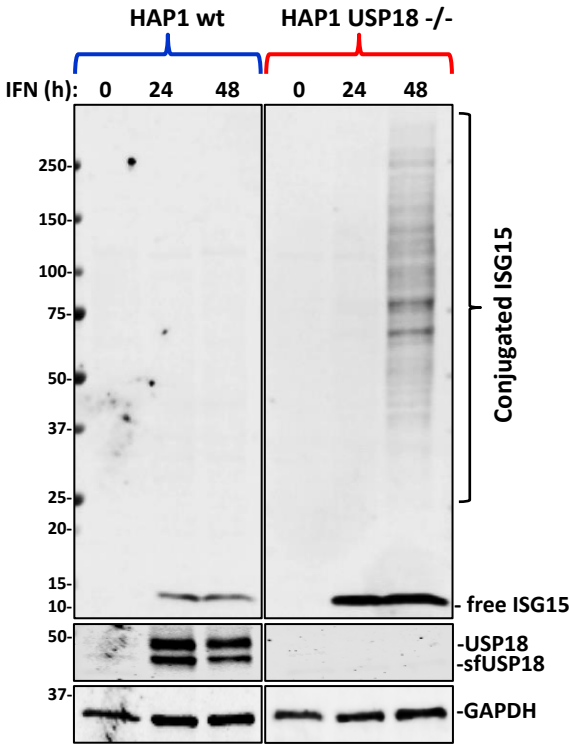
C



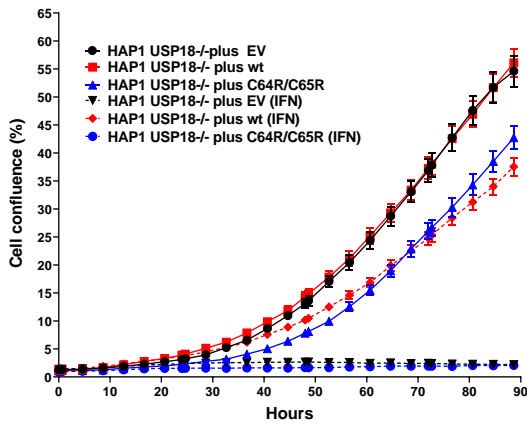
D



E



F



G

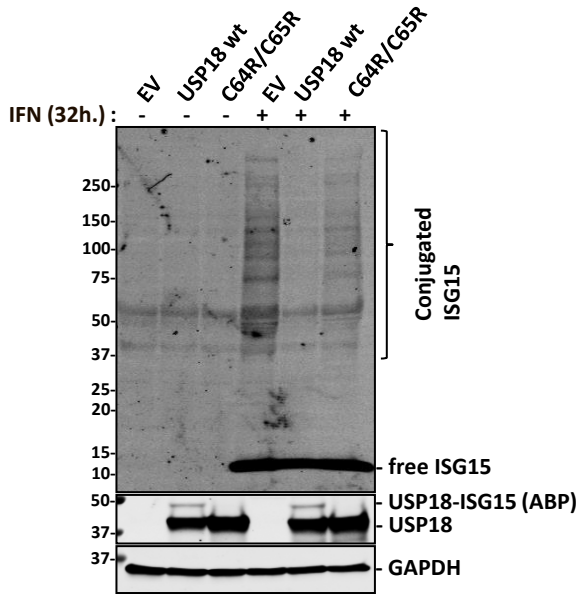
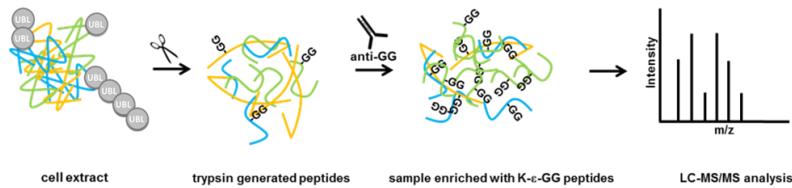


Figure 2

A GlyGly peptidomics workflow

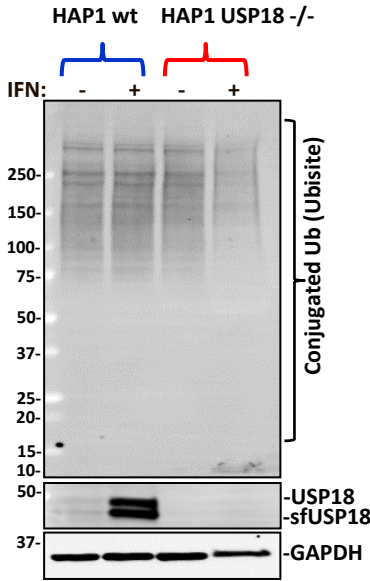


\*UBL = Ub, NEDD8 and ISG15

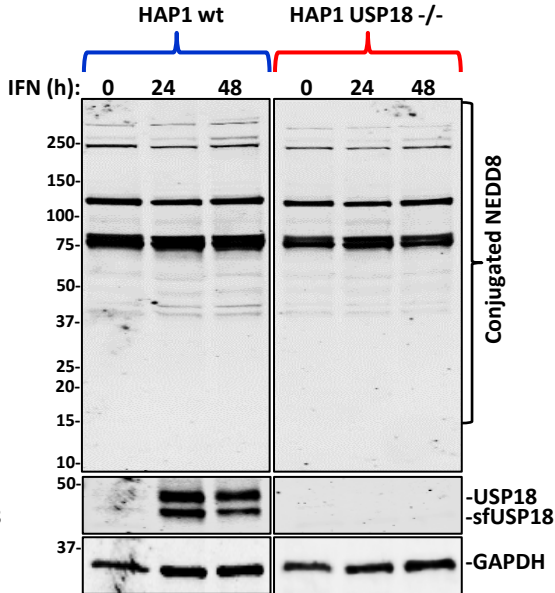
B

UBL	C-terminal motif
Ubiquitin	LRLRGG
NEDD8	LALRGG
ISG15	LRLRGG
SUMO1	QEQTGG
FAT10	CYCIGG

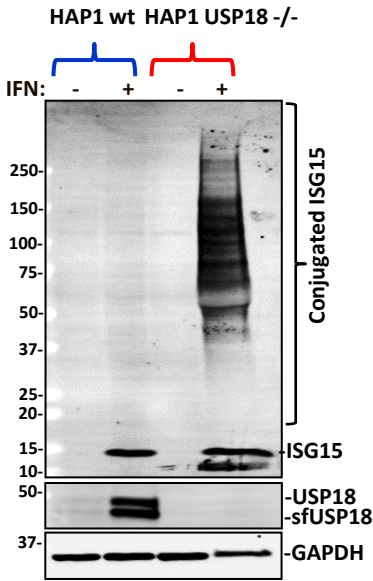
C



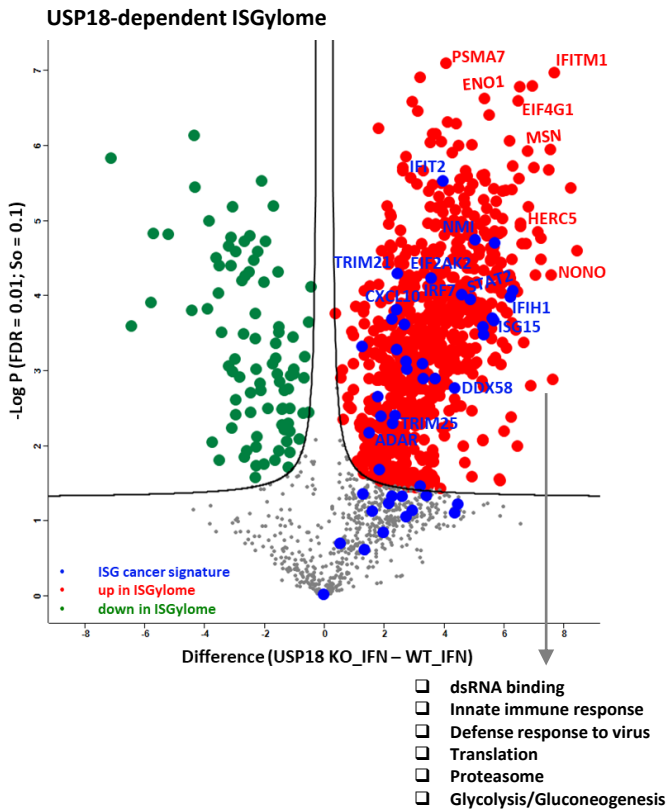
D



E



F



G

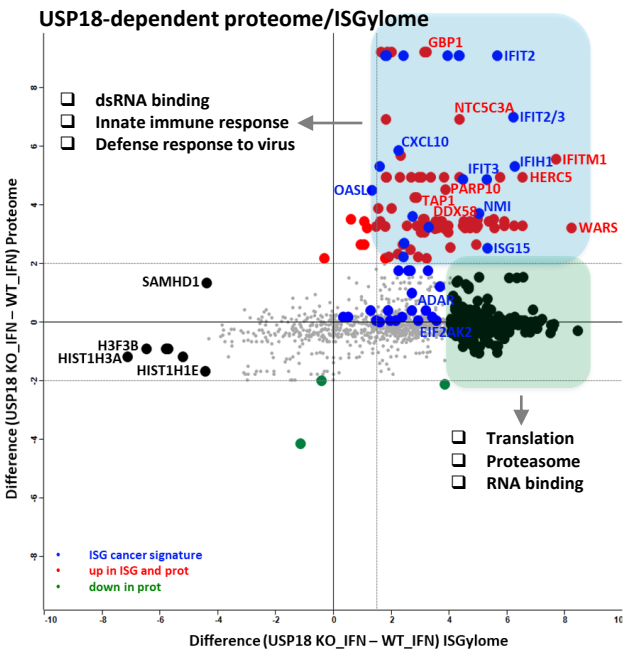
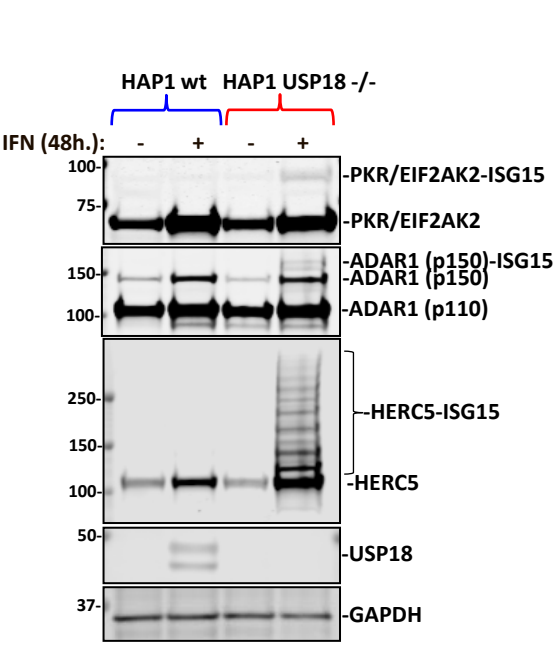
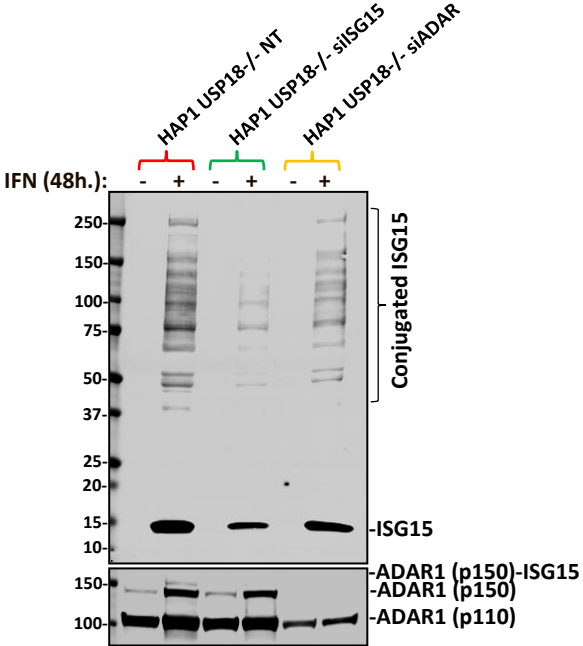


Figure 3

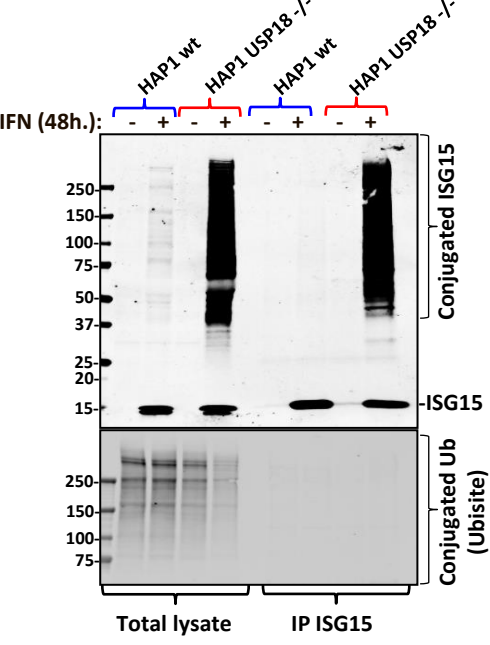
A



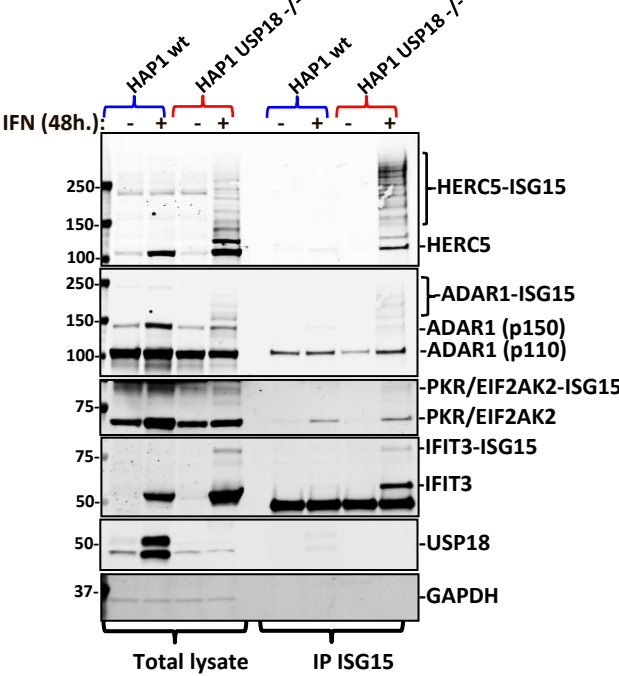
B



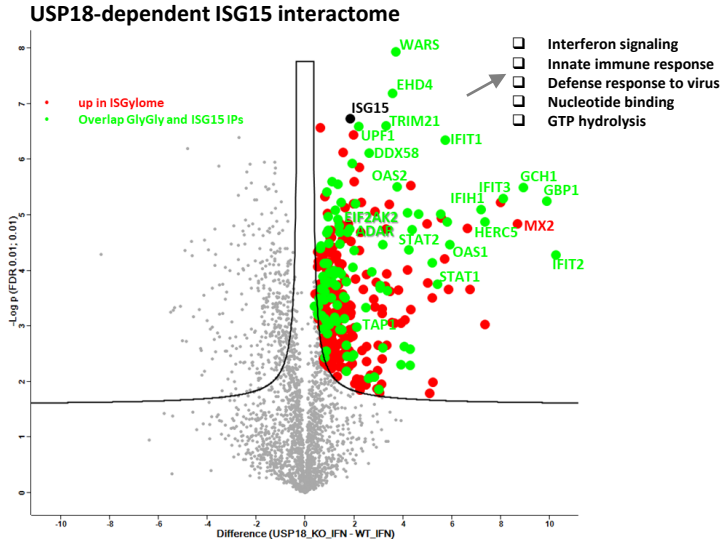
C



D



E



F

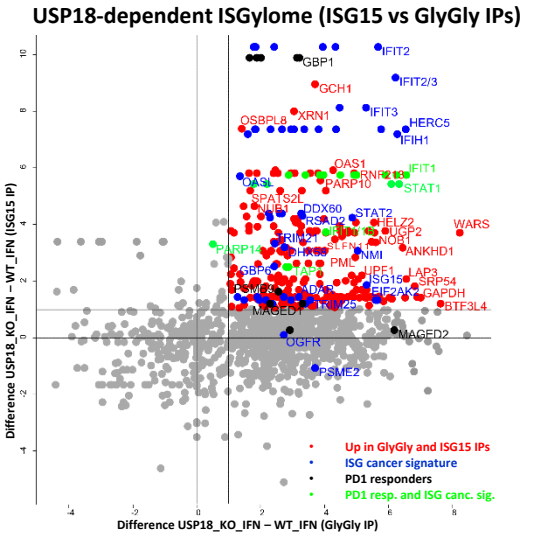
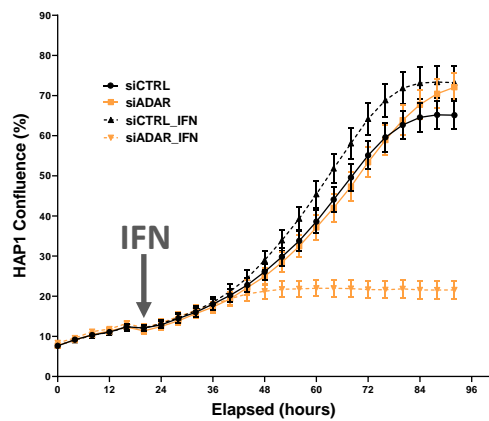
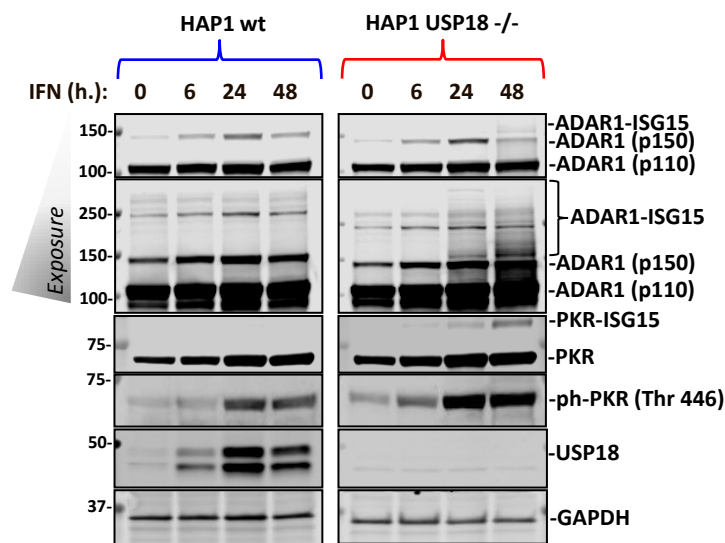


Figure 4

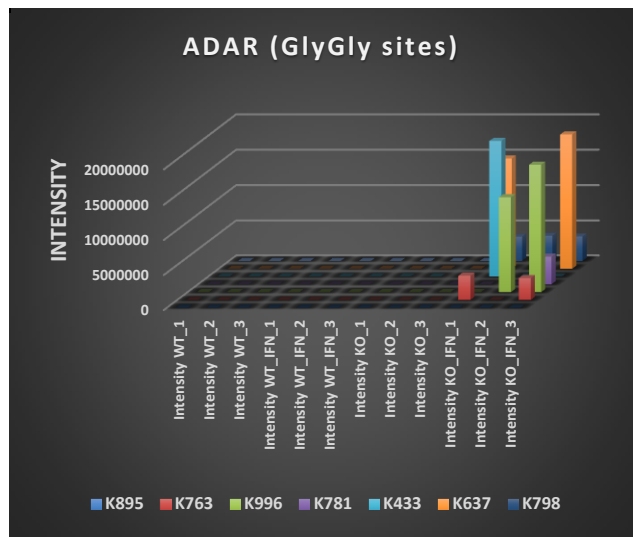
A



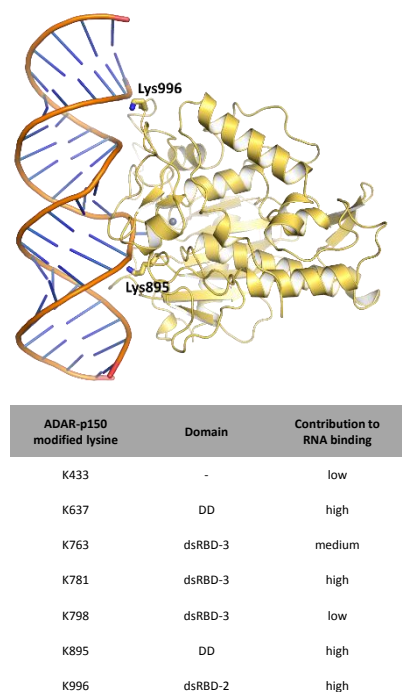
B



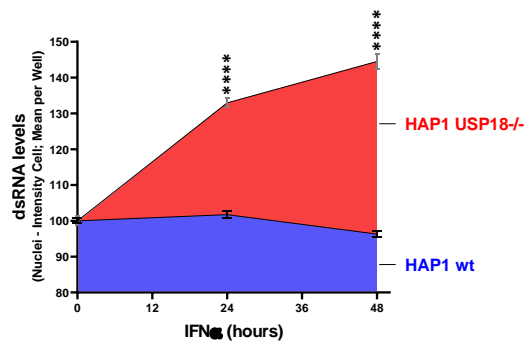
C



D



E



F

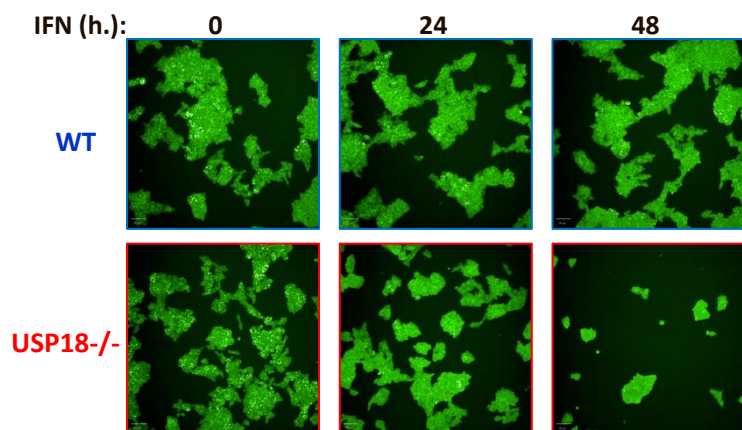


Figure 5

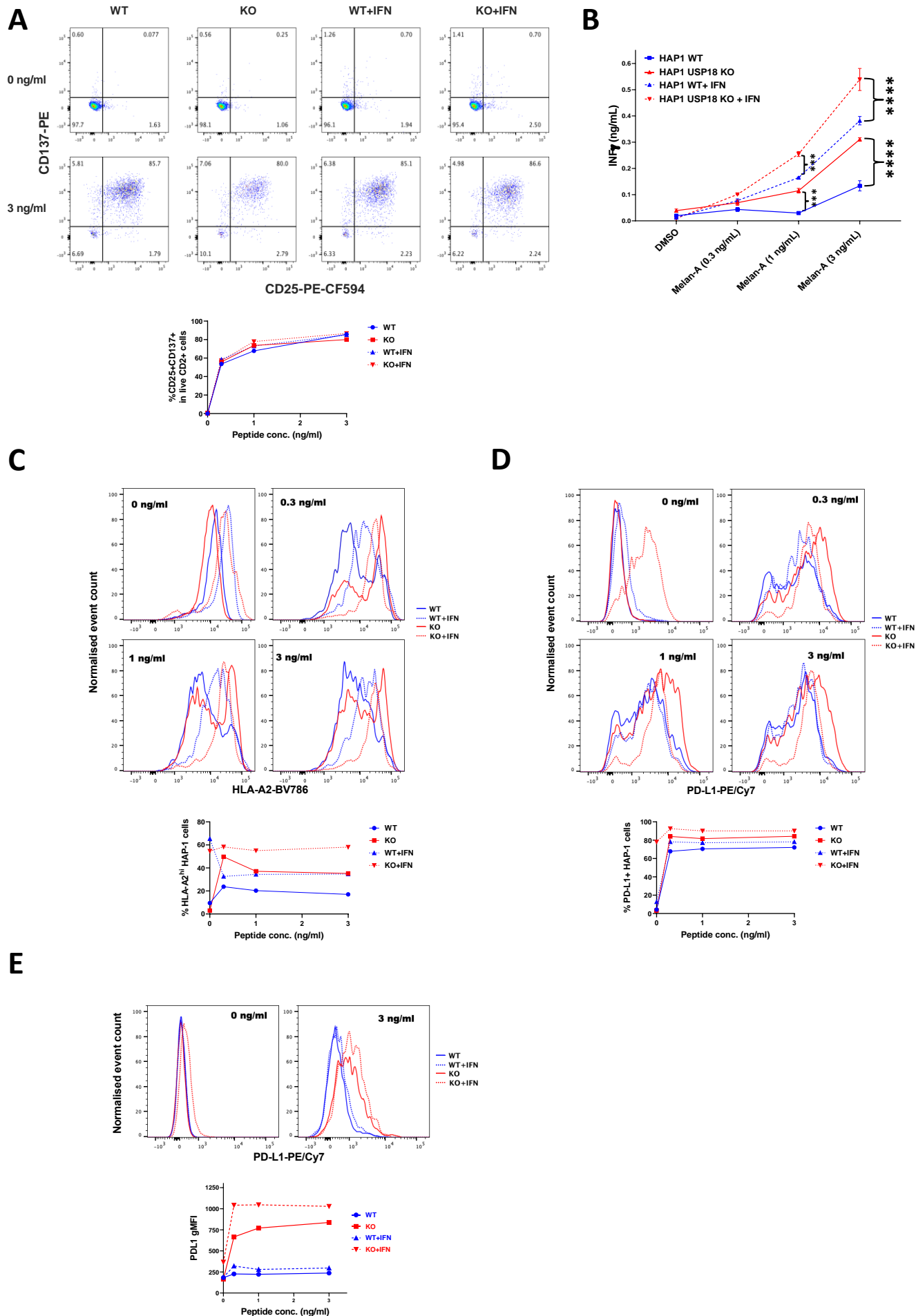
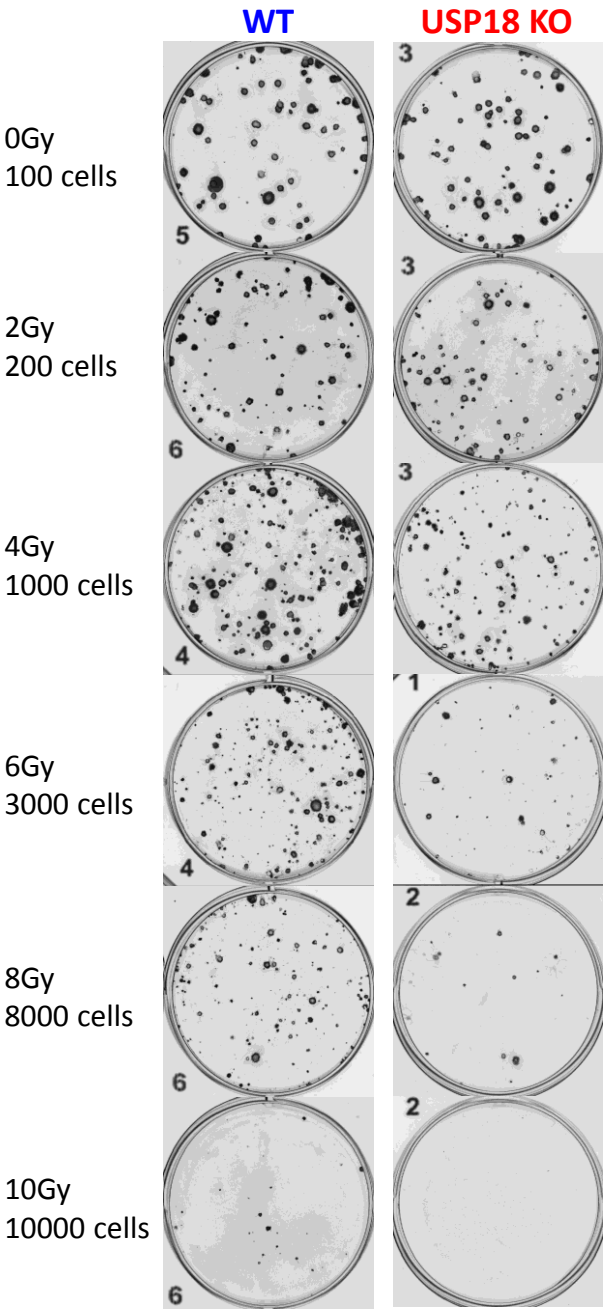


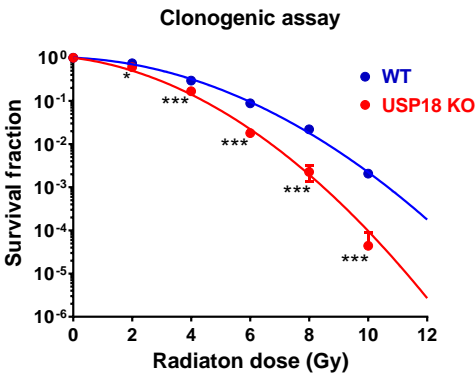
Figure 6

A

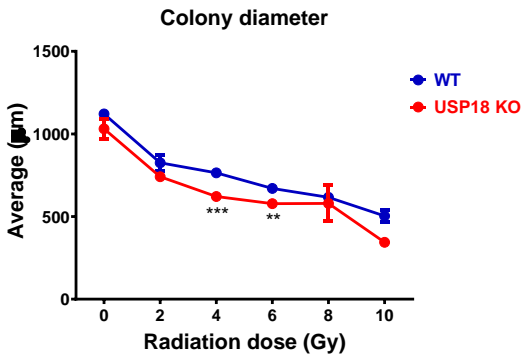
IR dose  
Seeding cell number



B



C



D

